DEUTSCHES ELEKTRONEN-SYNCHROTRON **DESY**

DESY 88–143
FTUAM-EP-88-07
September 1988

Top Search Strategies for HERA

G. Ingelman, G.A. Schuler
Deutsches Elektronen-Synchrotron DESY, Hamburg

J.F. de Trocóniz
Universidad Autónoma de Madrid, Madrid

ISSN 0418-9833

NOTKESTRASSE 85 · 2 HAMBURG 52

To be sure that your preprints are promptly included in the
HIGH ENERGY PHYSICS INDEX ,
send them to the following address (if possible by air mail) :

DESY
Bibliothek
Notkestrasse 85
2 Hamburg 52
Germany

DESY 88–143
FTUAM-EP-88-07
September 1988

ISSN 0418-9833

Top Search Strategies for HERA

G. Ingelman, G.A. Schuler
Deutsches Elektronen-Synchrotron DESY
Notkestrasse 85, D-2000 Hamburg 52, FRG

J.F. de Trocóniz
Universidad Autónoma de Madrid, Madrid, Spain

Abstract

We investigate strategies for a top quark search to be performed in *ep* collisions at the HERA energy. Signatures based on both the semileptonic and non-leptonic decay modes of the top flavoured hadrons are investigated and compared with detailed calculations of all relevant background processes. The study is based on Monte Carlo simulation of complete events making an experimentally realistic study possible. Clean top samples can be obtained, but a delicate choice of cuts is required in view of the small event rate expected for top quark production. We demonstrate that top events can be selected and observed up to a top quark mass of about 80 GeV, but a proper mass reconstruction is limited to 60–70 GeV.

1 Introduction

The existence of a sixth quark, called top, is expected in order to complete the three-family structure of quarks to correspond to that of the leptons. The top quark mass cannot, however, be well constrained theoretically and hence a relatively large range in mass must be considered. The experimental efforts to discover the top quark have so far only given negative results which are expressed in terms of lower bounds on its mass. A direct top search in $p\bar{p}$ collisions performed by the UA1 collaboration [1] at the CERN SPS collider gives the presently highest such bounds, namely $m_t > 44$ to 56 GeV depending on uncertainties in the theoretical cross-section calculations used. A similar bound is obtained more indirectly through B^0–$\bar{B}^0$ mixing observed by the ARGUS collaboration [2], indicating that the top quark mass is probably larger than about 50 GeV. The safest bounds originate from e^+e^- annihilation experiments but are limited by the centre-of-mass energies available in such machines. Thus, PETRA experiments give the limit $m_t > 23$ GeV [3] and the absence of an increase in R at TRISTAN pushes this limit to 26 GeV [4].

Future top searches may be performed with increased statistics at the CERN $p\bar{p}$ collider as well as at higher energies at the Tevatron. This may lead to a discovery or still higher bounds on the mass, but the major problem of very large backgrounds makes the top search increasingly difficult at hadron colliders. In e^+e^- annihilation at SLC and LEP I a top quark can be directly observed only up to a mass of 45–50 GeV; a region that already seems excluded from the above limits. Before still higher energies will be available in e^+e^- and $p\bar{p}$ machines, there will also be a new possibility through high energy *ep* collisions in HERA at DESY. With a 30 GeV $e^\mp$ beam on 820 GeV protons, giving $\sqrt{s} = 314$ GeV, a promisingly large cross-section for top production has been predicted through the boson-gluon fusion mechanism [5,6]. Although *ep* collisions are not as clean as e^+e^- interactions, there are considerably fewer processes occuring compared to the 'messy' $p\bar{p}$ collisions and the background problems are therefore expected to be less severe. This gives an opportunity for HERA to discover the top quark, provided that its mass does not exceed $\sim$ 85 GeV in which case the event rate becomes too small.

In a previous paper [7] we have studied the main characteristics of charm, bottom and top production in *ep* collisions. It was shown that the typical charm and bottom events are different from the top events in some observables. However, the many order of magnitude larger cross-sections for charm and bottom production lead to tails in the crucial distributions which prevent the selection of top events by cuts in simple global observables. It was thus clear that a dedicated and much more detailed study is needed in order to find suitable criteria to select top events from a huge background, which also receives important contributions from processes involving light quarks. The purpose of this paper is therefore to critically examine various strategies for a top quark search in *ep* collisions at the HERA energy in order to assess which signatures and selection criteria might be useful. For this purpose we use a detailed Monte Carlo model [8] to simulate the top production mechanism. Complete events are simulated, not only for the top signal, but also for all relevant background processes in order to facilitate an experimentally realistic study of the problems involved in a top search. We start, in section 2, with a description of the processes giving the top signal as well as those processes which are expected to give a possible background. The total rates are given to show what factors the top event selection criteria must overcome to give a useful signal-to-background ratio. Lepton signatures are well-known and often used tags for heavy flavour events. The applicability of such signals in this case is studied in section 3. Due to the limited semileptonic branching ratio it is worthwile to examine which signatures are useful for the non-leptonic decay modes of the top quark; our results in this sector are given in section 4. Finally, in section 5, we summarize and discuss our results.

2 Processes and total rates

Heavy quark production can occur in *ep* collisions already in the leading order quark-parton model (QPM) through the charged current process $e + q \to \nu + Q$, Fig. 1a. As shown in

[7], the cross-section is tiny due to the smallness of the Cabibbo-Kobayashi-Maskawa matrix elements for mixing between the top quark and the light quarks, that occur abundantly in the proton. The QPM process can therefore be neglected in comparison with the dominant production, which is found to be the boson-gluon fusion process

$$V(q) + g(p) \rightarrow Q_f(p_f) + \bar{Q}_{f'}(p_{f'}) \tag{1}$$

This is the next-to-leading parton level subprocess of the order $\mathcal{O}(\alpha_s\alpha^2)$ ep scattering process

$$e^{\pm}(l_e) + p(P) \rightarrow l'(l') + Q_f(p_f) + \bar{Q}_{f'}(p_{f'}) + X \tag{2}$$

shown in Fig. 1b. The process is here written for the production of a heavy quark (Q) of any flavour (f) to be generally applicable for charm, bottom and top, all of which will be needed in our study. The symbols in brackets denote the corresponding 4-momenta. In the charged current (CC) case V, in eq. (1), is the $W^{\pm}$-boson whereas in neutral current (NC) interactions V corresponds to γ/Z^0 exchange and the produced quark and antiquark have the same flavour f. The cross section

$$\sigma(e^{\pm}p \rightarrow lQ\bar{Q}'X) = \int dy \int dQ^2 \int dx_g \int dz \int d\Phi \; g(x_g, M_g^2)\hat{\sigma}(y, Q^2, x_g, z, \Phi) \tag{3}$$

is a convolution of the gluon density $g(x_g, M_g^2)$ and a cross-section $\hat{\sigma}$ for the parton level subprocess which takes proper account of the heavy quark masses and the complete electroweak structure for both charged and neutral current processes with γ/Z^0 interference [5].

The normal deep inelastic scattering (DIS) variables

$$Q^2 = -q^2 = -(l_e - l')^2 \;, \;\; x = \frac{Q^2}{2P \cdot q} \;, \;\; y = \frac{P \cdot q}{P \cdot l_e} \;, \;\; W^2 = (P+q)^2 \tag{4}$$

(out of which only two are independent) enter eq. (3) together with three new variables to completely specify the process in eq. (2). These additional independent variables are chosen as the gluon momentum fraction x_g, defined by $p = x_g P$, and an internal variable $z = P \cdot p_f / P \cdot q$ for the $Q\bar{Q}'$ system (related to the angle between the $Q\bar{Q}'$-axis and the boson-gluon axis) and the azimuthal angle Φ between the lepton and hadron planes, see [7] for details. We note that the gluon momentum fraction is related to the usual Bjorken-x variable by

$$x_g = x + \frac{\hat{s}}{ys} \geq x \tag{5}$$

where, as usual, $\hat{s} = (p_f + p_{f'})^2$ and $s = (l_e + P)^2$ denote the squared invariant masses of the $Q\bar{Q}'$-subsystem and the complete ep system, respectively.

For the numerical evaluation of the cross-sections we use the gluon structure function parametrization EHLQ1 [9]. Details of parameter values are given in [7] as well as a discussion of the uncertainties of the calculated cross-sections. These are found to be rather small for top production, $\lesssim$ 30%, but larger for charm and bottom due to less well-defined quark masses (current or constituent) and the larger uncertainty of the gluon distribution at small x. We note that our choice of $\hat{s}$ as the scale for α_s and the gluon density, M_g in eq. (3), is the largest realistic scale and therefore gives a rather conservative estimate for the top production cross-section. Using the smallest realistic scale, $(m_t/2)^2$, leads to a factor two

larger cross-section for both neutral current $t\bar{t}$ and charged current $\bar{t}b$ production. To reduce this uncertainty the full order α_s^2 corrections are needed.

The variation of the top quark production cross-section with its mass is given in Fig. 2. The NC process is strongly dominated by pure γ exchange and receives its main contribution at very small Q^2, i.e. essentially real photoproduction [7]. For $m_t \lesssim 55$ GeV the CC process dominates due to the smaller threshold associated with single top quark production ($\bar{t}b$) in comparison to pair production ($t\bar{t}$) in NC. The total inclusive top cross-section, defined by

$$\sigma_t = 2\sigma(ep \rightarrow et\bar{t}X) + \sum_f \sigma(ep \rightarrow \nu t\bar{q}_f X) \;, \tag{6}$$

shows that a top search at HERA seems possible up to $m_t \approx 85$ GeV where the rate is still about 10 events for an integrated luminosity of 200 pb^{-1}, which corresponds to a year of data taking under good conditions. In our following analysis we use the three top quark masses 40, 60 and 80 GeV to illustrate the three different regions where NC production dominates, NC and CC are of equal importance and CC interactions dominates, respectively. The main part of the analysis is performed for $m_t = 60$ GeV, which is thus our standard choice used unless otherwise stated.

Turning now to the possible background processes we first note that charm and bottom production through the same boson-gluon fusion mechanism, eqs. (1,2), provides serious background problems [7]. These occur naturally through decay leptons, but also in purely hadronic signatures like energy flows and event shape measures. The main contributions are $b\bar{b}$ and $c\bar{c}$ production which occur dominantly through photon-gluon fusion at low Q^2, but also $\bar{c}s$ production in charged current W-gluon fusion. We use the Monte Carlo model AROMA 1.2 [8] to simulate all heavy flavour processes. The model is based on the following main ingredients: *(i)* The complete matrix elements to order $\alpha^2\alpha_s$ for the boson-gluon fusion process [5] (including the masses of the produced heavy quarks and the full electroweak structure of the interaction), *(ii)* gluon emission from the $Q\bar{Q}'$ system in a parton cascade approach [10] and *(iii)* hadronization with the Lund string model [11] and heavy flavour decay. We emphasize that the parton cascade gives rise to multi-jet final states. For example, $b\bar{b}g$ events are obtained which are expected to be a main background to the signature based on an isolated lepton plus a jet.

The background from other processes, not involving heavy flavours, is naturally divided into NC and CC contributions. The neutral currents have a large cross-section at small Q^2 and it is for practical reasons convenient to treat the low-Q^2 region separately from the deep inelastic region. The latter we define by $Q^2 > 4$ GeV^2 where the DIS formalism can be safely applied and structure function parametrizations usually start their Q^2 evolution.

The cross-section at Q^2 close to zero is dominated by interactions that can be described in the VDM approach [12]. The close to on-shell photon does here appear as a virtual vector meson (ρ^0) which interacts strongly with the proton. This gives dominantly rise to minimum bias events, without large transverse momenta, which will not be of importance as a background for top events since a major requirement in any top search will be a substantial transverse activity. Large $p_\perp$ interactions at low Q^2 are properly described through the order $\alpha\alpha_s$ parton level processes of photon-gluon fusion and gluon radiation (QCD Compton), i.e.

$$\gamma + g \;\; \rightarrow \;\; q + \bar{q} \tag{7}$$

$$\gamma + q \;\; \rightarrow \;\; q + g \tag{8}$$

where q is any light quark (u, d, s or antiquark). Of course, the same kind of interactions also occur through weak boson exchange (except for flavour mixing in the CC case), but their rates are much smaller at low Q^2. Nevertheless, the complete structure for both γ/Z^0 and $W^\pm$ exchange at an arbitrary Q^2 are implemented in AROMA for these processes. In order to avoid the soft and collinear divergences in the matrix elements we apply a cutoff in the quark transverse momentum,

$$\text{for light quark processes}: \; p_\perp > 1 \; GeV. \tag{9}$$

As for the heavy flavour production, we take additional gluon radiation into account by applying a parton cascade in the final $q\bar{q}$ and qg states. The final parton state will therefore include not only additional gluons but also quark-antiquark pairs from gluon splitting, i.e. $m \times g + n \times q\bar{q}$ with $m,n = 0,1,2....$

The deep inelastic region we define by

$$\text{DIS region}: \; Q^2 > 4 \; GeV^2 \; , \; x > 10^{-3} \text{ and } W^2 > 5 \; GeV^2 \tag{10}$$

and simulate such events with the Monte Carlo program LEPTO 5.2 [13] which is based on the leading order electroweak cross-sections for ep scattering via γ/Z^0 and $W^\pm$ exchange. QCD corrections are taken into account via a parton cascade treatment in this case also, but using a scheme developed especially for DIS and which takes both initial and final state radiation into account [14]. Thus, the quark may radiate gluons both before and after it is struck by the exchanged boson and, as before, the gluons may also split into $q\bar{q}$ pairs. In both AROMA and LEPTO the parton states are hadronized using the Lund string model [11,10] including a phenomenological treatment of the target remnant partons [15,13] in order to simulate complete final states. Although the cross-sections for these large Q^2 processes are much smaller than for the low Q^2 processes above, they cannot be neglected in a top search as will become clear in our following analysis.

Clearly, there is an overlap between the two Monte Carlo programs and a double counting of processes and cross-sections must be avoided by running them under proper conditions and in complementary phase space regions. In particular, to avoid double counting of heavy flavour production, which are studied separately as described above, we restrict the number of flavours given by proton structure function parametrizations to three. Similarly, for the parton cascade simulation, only gluon splitting into light $q\bar{q}$ pairs is allowed, but not into charm and heavier. The complementary nature of the two programs provides, on the other hand, some possibilities for cross-checks. This is particularly important for the treatment of higher order QCD processes. As will be seen below, the multiple parton emission in the background processes is of great importance since our top signatures will typically include a requirement of a minimum number of jets. Without multiple parton emission the background processes could easily have been rejected and a clean sample of top events with multiple jets originating from the top quark decay would remain. This would, however, have been an unrealistically favourable situation that cannot be accepted in a detailed study of top search strategies.

A comparison of the cross-sections for the top signal and the various background processes is given in Table 1. Clearly, the about 7 orders of magnitude larger background cross-section

makes it quite clear that extremely powerful signatures are needed in order to extract a reasonably clean top sample. Also given in Table 1 are general characteristics of top and background events in terms of the mean values of the total transverse energy, $\sum E_\perp$, the transverse sphericity or 'circularity', C as defined in section 4, and the charged particle multiplicity, n_{ch}. Here, and always in the following, an angular cut has been applied to exclude particles with angles $\theta < 5.7°$ with respect to the beam directions, since they will not emerge from the beam pipe and are hence not measurable. One may have expected that the top events should be more spherical, due to the top decay, but since the lighter flavours are dominantly produced close to threshold they also tend to have a similar circularity. Hence, there is no discriminating power in this observable when applied to an inclusive event sample [7]. Although the mean charged multiplicity is somewhat larger in top events, as expected, the distributions are rather wide and the difference is therefore not large enough to be very useful. Multiplicities are, furthermore, not so easily measured since a track reconstruction is required.

The total transverse energy, on the other hand, is more directly obtained from the energy measurement in the calorimeter. Since we are primarily interested in the hadronic final state we have here excluded the scattered lepton, which is either unmeasured (CC and low Q^2) or a well isolated high-$p_\perp$ electron that can be identified. As shown in Table 1, the mean $\sum E_\perp$ is considerably larger for top events compared to most background processes and therefore provides the first inclusive way to reduce the background. To be more specific the distributions in $\sum E_\perp$ for top and background events are compared in Fig. 3. All stable (charged and neutral) particles outside a beam pipe cut of 5.7° are included to correspond to a global measurement in a calorimeter. As expected from the large transverse momenta of the top quarks [7] and the large energy release in their decay, top events give rise to a wide distribution. In contrast, the backgrounds peak at small $\sum E_\perp$, but have tails to large $\sum E_\perp$ which are in fact above the top signal. Nevertheless, a cut in this quantity is very efficient to improve the signal-to-background ratio; the background can be reduced by several orders of magnitude without any substantial loss of top events.

The large $\sum E_\perp$, occuring also in background events, arises through two different sources of transverse momenta. The first is generated in hard QCD processes such as gluon radiation and photon-gluon fusion. This leads to the normal power-behaved distribution in parton $p_\perp$, measured with respect to the axis of the colliding boson-parton system in its cms frame. It is important to note, however, that heavy quark production is damped in this way only for $p_\perp \gtrsim m_Q$ [7]. In DIS the scattered lepton emerges with a transverse momentum

$$p_\perp^2 = Q^2(1-y) \tag{11}$$

(independent of the quark mass) which is balanced by the hadronic system through the exchanged boson. This latter source can only be neglected for photoproduction, i.e. $Q^2 \to 0$, but not otherwise. Although the NC cross-section decreases with increasing Q^2, the cross-section remains large enough to give a non-negligible rate of events with large $\sum E_\perp$ originating from this kinematical source. Together with the QCD $p_\perp$-source this creates the tails to large $\sum E_\perp$ in Fig. 3. The CC cross-section is dominated by large Q^2 and therefore lacks the strong peaking at small $\sum E_\perp$, resulting in a wider distribution with a larger mean value. Clearly, for a top search one cannot consider photoproduction only, since important background processes are present in the DIS region at large Q^2.

For the following analysis, of both the semileptonic and non-leptonic top decay modes, we apply some general cuts. To take the acceptance loss due to the beam pipes into account we disregard all particles closer than 5.7° to the beam directions. A cut in $\sum E_\perp$ is clearly very powerful and we will always require a minimum of 20 GeV. When the analysis is directed towards $t\bar{t}$ events this can be increased to between 40 and 80 GeV. From the discussion above on the contributing sources to background events with large $\sum E_\perp$ it is clear that one would like to exclude large Q^2 events. For the neutral current process this can be done rather straight-forward since they should have a clear experimental signature with the high-$p_\perp$ scattered electron well separated from the balancing hadronic system in the opposite azimuthal hemisphere of the detector. To assure a correct event identification [16] one can furthermore check the matching of the kinematical variables measured from the scattered electron and from the hadrons. Since NC production of top is strongly dominated by low Q^2, this signal need not be appreciably affected. Thus, for NC events we reject events with $Q^2 > 10$ GeV^2, where the electron is at a large enough angle and $p_\perp$ to be identified. This leads, however, to a $\sim 25\%$ loss of $t\bar{t}$ events (see Fig. 4a in [7]). Such a cut is of no use for charged current processes since it would seriously reduce the CC top production, which is dominant at large Q^2. In summary, the generally applied cuts are

$$\theta > 100\,mrad\,,\ \sum E_\perp > 20\,GeV\,,\ \left\{Q^2 < 10\,GeV^2 \text{ for NC}\right\}. \qquad (12)$$

Starting from these we now investigate which further criteria are useful to extract top event samples.

3 Semileptonic analysis

Leptons from semileptonic heavy quark decays provide a standard way to tag heavy flavour production in different interactions. Due to the sequential top decay $t \to b \to c$ there is a large probability for having a lepton in the final state of top events. In fact, there is a non-negligable probability for two or more leptons, in particular in $t\bar{t}$ events, which may in itself provide a top signature. From the large cross-sections for $b\bar{b}$ and $c\bar{c}$ production it is, however, clear that additional requirements are necessary to filter out top events from charm and bottom. The decreasing mass in the sequence top-bottom-charm leads to decreasing transverse momenta and thereby also less well isolated leptons from the corresponding quark decays. Cuts in lepton $p_\perp$ and isolation are therefore natural possibilities. Ideally the transverse momentum should be measured with respect to the direction of the decaying heavy quark momentum vector. The latter is, however, very difficult to reconstruct experimentally. One can therefore use the lepton $p_\perp$ w.r.t. the beam axis since this should reflect the decay dynamics, although it will also obtain contributions from the QCD and DIS $p_\perp$ sources discussed above. The increasing scale of the quark transverse momentum with its mass, as shown in [7], contributes further to an expected characteristically higher $p_\perp$ of leptons in top events. Concerning lepton identification, muons do not pose any serious problem, but electrons cannot easily be identified in a hadron environment and an isolation criterion is therefore prefered also from an experimental point of view.

3.1 Dilepton signature

For the dilepton signature we simply require a pair of leptons and include both muons and electrons in order to gain in rate. A requirement of both leptons to be isolated from hadrons would strongly reduce the rate and is therefore not made. This poses an experimental problem for electrons which may, however, be solved by electron-hadron separators like transition radiation detectors or silicon detectors in the calorimeter. Since a requirement of two leptons tend to favour $t\bar{t}$ events over $\bar{t}b$ events it is reasonable to increase the transverse energy cut as is clear from Fig. 3. We thus choose $\sum E_\perp > 40$ GeV as a compromise to reduce the backgrounds but still keep the major part of the $\bar{t}b$ events.

With these criteria, and the general cuts in eq. (12), the results in Fig. 4 and Table 2 are obtained. The scattered electron in NC events is not included in these lepton pairs since it is either at a very small angle and escapes detection or it can be identified as argued above and therefore removed. Fig. 4a shows the cross-section as a function of a lower cut in $p_\perp$ of the highest-$p_\perp$ lepton in the pair. For background events including light quarks only, the leptons are electrons and positrons from particle decays, such as π^0 Dalitz decays. If only di-*muon* pairs would be considered this background would be absent, but of course all other dilepton cross-sections would be reduced by a factor four. Since the dominant background at non-zero $p_\perp$ is given by $c\bar{c}$ and $b\bar{b}$ production, which also contains muons, this is of no advantage. It is clear from Fig. 4a that a cutoff in the lepton $p_\perp$ has to be applied in order to reduce this background. From Table 2 the ratio of the total signal $(t\bar{t} + \bar{t}b)$ to the total background is found to be $(26, 2.5, 0.6) \times 10^{-3}$ for $m_t = (40, 60, 80)$ GeV if no cut in $p_\perp$ is applied, but it improves to $(0.59, 0.069, 0.017)$ if one lepton is required to have $p_\perp > 10$ GeV. With this cut applied, Fig. 4b shows the variation of the cross-section with a cutoff in $p_\perp$ of the other lepton. Although the signal-to-background ratio can be improved somewhat, e.g. to $(0.85, 0.10, 0.021)$ with the second lepton having $p_\perp > 5$ GeV, there is no possibility of a drastic improvement this way. Cuts in other observables might be more effective, but have not been investigated yet.

Nevertheless, in the case of a light top quark, e.g. 40 GeV, a signal-to-background ratio of order unity can be obtained with decent statistics, e.g. 40 top events in 200 pb^{-1} using the cut $p_\perp^{cut_1} > 12$ GeV. For a top mass larger than 50–60 GeV, such a signal-to-background ratio can only be obtained at the prize of a considerably smaller absolute rate when only lepton $p_\perp$ cuts are used. A better result might be obtained with less severe lepton cuts in combination with cuts in other kinds of observables.

3.2 Isolated-lepton signature

The cross-section for events satisfying eq. (12) and having a lepton (electron or muon) with a transverse momentum larger than a lower cutoff, $p_\perp^{cut}$, is shown in Fig. 5. (For events with more than one lepton the highest-$p_\perp$ lepton is taken.) As can be seen the charm and bottom backgrounds dominate the cross-section out to very large lepton $p_\perp$. Also the background from light quark events, in particular CC, is above the top signal for lower lepton $p_\perp$. To obtain a reasonably clean top sample a very large $p_\perp^{cut}$ would have to be applied, but this would reduce the rate too much. As a reasonable compromise we choose $p_\perp^{cut} = 8$ GeV and

instead try to improve the purity of the top sample by cuts in other observables. The large top quark mass imply a large energy release in its decay and consequently leptons from such decays are expected to be well separated from other decay products and presumably also from other particles in the event. We emphazise that a realistic estimate of this expectation can only be obtained from complete event simulation such as in our Monte Carlo models. To investigate lepton isolation criteria we define the accompanying energy as the energy within a cone of half-'angle'

$$\Delta R \equiv \sqrt{(\Delta\eta)^2 + (\Delta\phi)^2} \leq R_c \tag{13}$$

where $\Delta\eta$ and $\Delta\phi$ are the distances to the lepton in laboratory pseudorapidity and azimuthal angle (around the beam). A lepton is then said to be isolated if the total transverse energy, E_{acc}, within the cone is less than a given minimum value, E_{acc}^{cut}. After having verified that the isolation criterion is rather insensitive to reasonable variations of R_c we have chosen $R_c = 0.4$. The variation of the cross-section with the accompanying energy is shown in Fig. 6. A suitable cut is seen to be $E_{acc} \leq 1$ GeV, since the charm and light quark backgrounds are then suppressed far below an almost unchanged top signal. The remaining background is $b\bar{b}$ events, which are considerably reduced by this cut, but are still about two orders of magnitude larger than the top signal.

Semileptonic decays of heavy quarks are also characterized by the missing transverse momentum, $\not{p}_\perp$, carried away by the neutrino. An experimental measurement of $\not{p}_\perp$ can be made based on overall transverse momentum conservation, but will include other contributions as well. Other semileptonic decays than that producing the isolated lepton may be present and contribute escaping neutrinos. In CC events the scattered lepton is a neutrino and since the CC cross-section dominates at large Q^2 the resulting $\not{p}_\perp$ will be correspondingly large according to eq. (11). For NC events the scattered electron will only give rise to a small $\not{p}_\perp$ for small Q^2 when it escapes detection in the beam pipe due to a very small scattering angle. Many hadrons emerging at small angles will also be lost in the beam pipe and contribute to $\not{p}_\perp$. In a $p_\perp$ vector sum, however, they tend to cancel each other leaving a limited net $\not{p}_\perp$ which is taken into account by the minimum angle cut in eq. (12). Other experimental uncertainties that may enter depend on the detailed detector setup and are therefore not included in our analysis. The cross-section as a function of a minimum $\not{p}_\perp$ is shown in Fig. 7 for the isolated-lepton event samples obtained by the above criteria. The dominating $b\bar{b}$ background can be completely suppressed by a the requirement $\not{p}_\perp > 10$ GeV, without a significant reduction of the top signal.

In summary, we have found it suitable to define the isolated-lepton signature by

$$p_\perp^l > 8\ GeV \quad \text{and} \quad \sum E_\perp < 1\ GeV \ \text{ within } \Delta R < 0.4 \text{ of the lepton} \tag{14}$$

Together with the requirement

$$\not{p}_\perp > 10 \text{ GeV}$$

this completes the selection criteria for this analysis. The cross-sections and mean values of the main observables in this analysis are summarized in Tables 3 and 4, respectively. The results of the sequence of cuts are given in the different columns and it is thereby implicit that when moving from left to right the cuts in the previous columns are still applied. Thus, in Table 4 the cut in lepton $p_\perp$ is first applied and the mean accompanying energy is then given. A cut at 1 GeV is found to be appropriate, see also Fig. 6, and the mean missing transverse

momentum is thereafter given. No entry means that no Monte Carlo event survived the cuts and the cross-section is unmeasurably small. The combined effect of the cuts is, as summarized in Table 3, to reduce the top event sample ($t\bar{t} + \bar{t}b$) by a factor 4 to 6 depending on the top quark mass. In addition a 25–35% reduction arises due to the requirement of eq. (12) and, more important, a lepton in the final state, cf. Table 1 and 3. With these selection criteria and an integrated luminosity of 1 fb^{-1}, corresponding to five years full-time running of HERA, one would obtain $(260, 37, 10)$ ($t\bar{t} + \bar{t}b$) events for $m_t = (40, 60, 80)$ GeV, which should be compared with an estimated total background of about one event. Thus, a clean top sample can be obtained but at the cost of an overall factor 5–10 reduction in statistics. A non-vanishing sample requires, therefore, long running times with high luminosity. If this can be achieved, it is possible to probe the top quark up to a mass of about 80 GeV using this signature.

With samples defined in this way we now turn to the problem of an experimental determination of the top quark mass. The simplest hint is the rate of top events which, at the HERA cms energy, depends strongly on the top quark mass. This is illustrated in Fig. 8, where the cross-sections from Table 3 are converted to event rates as a function of the top quark mass. Clearly, the sensitivity to the top quark mass is only observable when the number of top events is larger than, or at least similar to, the number of background events surviving the cuts. Given the number of observed events a corresponding estimate of the top quark mass can be deduced from Fig. 8. For example, in case *(ii)* the observation of 200 events would lead to an estimate $m_t = 45 \pm 1$ GeV, whereas 20 events would correspond to $m_t = 75 \pm 4$ GeV at 68% statistical confidence level. The sensitivity of this top mass estimate depends both on the available statistics (i.e. vertical error bars in Fig. 8) and the slope of the error band. The latter reflects the strong mass dependence of the top production cross-section, but is affected by the applied cuts which tend to reject more top events in case of a lower mass. Case *(ii)* in Fig. 8 is rather optimal, since the background is already small and further cuts, like in *(iii)*, will reduce both the statistics and the slope of the error band and hence give a larger top mass error. The surprisingly high accuracy obtained from this method should not be misinterpreted. It is by no means a measurement of the top quark mass, but only an estimate. The result depends on uncertainties in the cross-section calculation as well as the detailed simulation of the response of signal and background events to the cuts applied in order to obtain the final event sample. Nevertheless, it will be very useful for the further analysis when a proper mass measurement is attempted.

The distributions of several observables also depend on the top quark mass and the question is which are sensitive enough to give useful information. The distributions in $\not{p}_\perp$ and $\sum E_\perp$ are shown in Figs. 9 and 10, respectively, for three values of m_t. The typical value of $\not{p}_\perp$ does increase with m_t, but not as strongly as the $\sum E_\perp$ one, as quantified by the mean values in Table 4. Thus, in particular the $\sum E_\perp$ distribution should be useful for an estimate of the top quark mass.

The final aim is, of course, to measure the top quark mass directly by a reconstruction of the top quark decay. This is, however, not possible for the $\bar{t}b$ events using the above leptonic signature since there are two neutrinos present, both usually with high $p_\perp$. One stem from the CC scattering itself and the other from the semileptonic decay, which is dominantly the top decay due to the isolation criterion. In the $t\bar{t}$ case, there is usually only one hard neutrino, from a top decay, whose transverse momentum can be obtained (or at least estimated) by

momentum conservation, i.e. identified with the measured $\not{p}_\perp$. The following topology (or its charge conjugate) is expected for the isolated-lepton $t\bar{t}$ sample

$$t \to b + l^+ + \nu_l \to \text{jet} + l^+ + \not{p}_\perp \ , \ \bar{t} \to \bar{b} + q + \bar{q} \to \text{jet} + \text{jet} + \text{jet} \qquad (15)$$

and the top quark mass could therefore be measured from both decay modes. In the non-leptonic decay one forms the proper invariant mass of the three jets, whereas in the semiletonic decay one can only obtain an estimate since the longitudinal momentum of the neutrino is not measurable. This momentum component can be neglected to obtain a top quark 'transverse mass' estimate, but a better approximation is obtained by using the value which minimizes the invariant mass of the $l + \nu + jet$ system [17]. We will therefore use this 'minimum mass' technique in the following.

To form these invariant masses we need to reconstruct jets. Since we work with complete event simulation models we can apply an experimentally realistic jet finding algorithm and choose one of the UA1 type based on the energy flow pattern as follows. A 'calorimeter' covers the full azimuthal angle around the beam axis and the pseudo-rapidity region $|\eta| \leq 3$, and is divided into cells of size $\Delta\eta \times \Delta\phi = 0.24 \times 12^\circ$ in which the particle energies are summed. Starting from the cell with largest transverse energy, nearby cells within a cone of half-angle $\Delta R \leq 0.7$ (see eq. (13)) are added and, if the summed transverse energy exceeds 7 GeV, this forms a jet with axis given by the $E_\perp$-weighted center of the cells. The procedure is iterated until all such jets are found. Fig. 11 shows the resulting jet multiplicity distributions for the background and signal events that survive the isolated-lepton criteria and have $\not{p}_\perp > 10$ GeV. We note that there are many three-jet configurations for the $t\bar{t}$ signal which means that one of the four expected jets in eq. (15) was either not resolved or lost due to limited acceptance. There are also configurations with more than the expected four jets. Since the top mass reconstruction analysis should only be done for $t\bar{t}$ events we have elevated the $\sum E_\perp$ cut to 60 GeV in order to reduce the $\bar{t}b$ contribution, which is rather a background for this purpose. The remaining $\bar{t}b$ background can be further suppressed by a requirement of at least 3 jets, which also deletes the remaining $b\bar{b}$ background but leaves most of the $t\bar{t}$ sample.

In order to perform the mass analysis of both the hadronic and semileptonic top decays in eq. (15) one would prefer a four-jet final state since this would directly correspond to the expected topology in eq. (15). A selection of four-jet events only would imply a serious loss of statistics, see Fig. 11. We therefore include all events with three or more jets, but apply *another* jet finding algorithm were the reconstruction is forced to give exactly four jets. This is achieved using LUCLUS [18] where particle pairs are joined into clusters as long as their distance d_{ij}, related to the transverse momentum within the pair, is smaller than a given resolution parameter d_{join}. The latter can be taken as a free parameter and the procedure is simply stopped when exactly four clusters remain. With these four jets the top mass can be calculated both for the semileptonic and non-leptonic decay mode as discussed above. The remaining problem is that one cannot *a priori* know which combination of jets, of the four possibilities, is the correct one. We have tried to resolve this ambiguity by investigating the topology of the events, but not found any useful method. We are therefore left with a combinatorial background also in the genuine $t\bar{t}$ sample. In Fig. 12 the resulting mass distributions are shown separately for the single right ($t\bar{t}_R$) and three wrong ($t\bar{t}_W$) combinations (known from the Monte Carlo) occuring for each event in the $t\bar{t}$ sample and the remaning contamination of $\bar{t}b$ events where this jet topology is not expected to give the

proper top quark mass. Backgrounds from events without top are too small to appear on this scale. The right combinations of reconstructed minimum 'leptonic' mass, $m_l = m(l\nu j)$, and the 3-jet 'hadronic' mass, $m_h = m(jjj)$, give both rise to nice peaks at the input mass of 60 GeV, but it is only in the latter case that the peak stand out above the combinatorial background within the top events themselves.

The dominant combinatorial background, as well as other backgrounds, can be further reduced by considering the two-dimensional distribution, $d^2\sigma/dm_l dm_h$, in the two reconstructed masses. These are given in Fig. 13, separately for background processes and the right and wrong combinations in $t\bar{t}$ events. As expected, it is only the correct combinations of jets in the $t\bar{t}$ events, Fig. 13d, that have a peak around the proper top quark mass, i.e. $m_l = m_h = m_t$. In all other cases a rather even distribution over the $m_l - m_h$ plane is obtained. A proper mass peak can now be clearly observed above the backgrounds and thus a top quark mass measurement be obtained from the position and width of the peak. By selecting only those combinations where the two reconstructed masses are in a window around the peak, e.g. $m_l \in [40, 65]$ GeV and $m_h \in [50, 65]$ GeV, and then making projections one can also obtain one-dimensional distributions in m_l and m_h where peaks in both these masses can be observed above the backgrounds. The cross-section for the jet combinations within this window is 15 fb. With an integrated luminosity of 1 fb^{-1} this corresponds to approximately 10 top events. The right combinations peak over the combinatorial background in a more restricted mass region; e.g. $m_h \in [58, 62]$ GeV, in the case of the 3-jet mass, which corresponds to a cross-section of 6 fb.

Another possibility to suppress the combinatorial background is to select only that combination of jets which minimize $|m_l - m_h|$. This should favour the right combinations of $t\bar{t}$ events, where both reconstructed masses should be close to the top quark mass. For the wrong combinations, however, such a symmetry between the two masses is not expected and they should therefore be disfavoured. This selection corresponds to a 'band' along the diagonal in Fig. 13 and has the advantage, compared to the window method above, that no explicit estimate of the top mass is needed. This would be more important in case a clear peak in the $m_l - m_h$ plane is not observed. The distributions in m_l and m_h, shown in Fig. 14, are the results obtained by selecting only the minimum $|m_l - m_h|$ combination in each event. Compared to Fig. 12, both mass peaks can now be clearly observed, and that without loss of statistics. It is noteworthy that, not only the 3-jet mass $m(jjj)$, but also the minimum mass, $m(l\nu j)$, peaks at the proper top quarks mass, $m_t = 60$ GeV. This proves the suitability of the jet reconstruction method used. In particular, forcing the reconstruction of exactly four jets implies that each event gives exactly one measure of both m_l and m_h. Consequently the integrated cross-sections in Fig. 14 a and b are equal, and have the value 14 fb, which can directly be translated in number of events. Since the peaks, in particular the one in $m(jjj)$, are well pronounced they contain the main part of this cross-section.

To summarise the top search based on the signature of an isolated lepton we have found the following main results. A clean top sample can be obtained up to a top mass of about 80 GeV at which point $\bar{t}b$ will dominate and, with the sequence of cuts that we found suitable, we expect about 2 events per 200 pb^{-1} integrated luminosity which can be obtained in a good year of HERA running. An estimate of the top quark mass can be obtained from the number of events passing the top selection criteria. The successful background suppression and the strong top mass threshold dependence at the HERA energy leads to a quite sensitive

mass dependence. Other observables, like the mean value of the total transverse energy, can also indicate the top quark mass. A proper mass reconstruction can only be made for the $t\bar{t}$ case and we have demonstrated that a mass peak can be extracted for a 60 GeV top quark. With a higher top mass value the signal-to-background ratio can be kept similar, but the rate is quickly reduced due to the strong threshold for $t\bar{t}$ production. Top candidate events would still be provided by $\bar{t}b$ events, but a direct mass measurement is not possible due to the presence of two neutrinos.

The successfully obtained mass peaks from $t\bar{t}$ events with $m_t = 60$ GeV were achieved by introducing some new and essential ideas. A predefined number of jets, corresponding to the expected top decay topology, are reconstructed to facilitate the combination of jets and leptons to form simultaneously the invariant masses of both the semileptonic and hadronic decay in the $t\bar{t}$ event. In the two-dimensional distribution of these masses the correct combinations of the jets give a peak which is above the more spread out combinatorial background. Thus, by requiring both these masses to be in a 'window' around this observable peak the remaining background is strongly suppressed also in the projected one-dimensional mass distributions and clear peaks emerge at the proper input top mass value. The latter is in itself a non-trivial result which relies on a proper jet reconstruction since losses of jets, due to acceptance or reconstruction inefficiencies, can easily distort the reconstructed mass value. The trick with a predefined number of jets is therefore proven useful since it does not create artificial jets which are unrelated to the expected top decay topology. A larger event sample, which would otherwise have been split into different jet multiplicities, are also accessible with this method. Naturally, the cuts applied reduce the statistics in the final mass plots and an expected rate of about 2 top events is expected for an integrated luminosity of 200 pb^{-1}. We emphazise, however, that the background is totally absent and that each event gives two top mass measurements, via the semileptonic and hadronic decay. Thus, the top quark mass can be uniquely reconstructed even with the relatively low rate expected. The statistics will furthermore be considerably larger after some years of data taking. For a heavier top quark this mass reconstruction method is simply limited by the $t\bar{t}$ event statistics. The practical limit seems to be at $m_t = 70$ GeV, where only 2 events per 1 fb^{-1} are expected.

4 Non-leptonic analysis

The top event sample complementary to the above analysis, i.e. without an isolated lepton, contains more statistics and it is therefore important to investigate its usefulness for a top search. From the Monte Carlo events we have verified that this sample almost coincides with those events where the top quarks actually decayed non-leptonically. Since there is no missing neutrino from the top decay the top mass reconstruction could be possible also for the $\bar{t}b$ case and should be favoured through the use of proper invariant masses obtained from fully measured jets without missing momentum estimates. In order to obtain a reasonably clean top sample some suitable selection criteria must be found. As mentioned in section 2, it is most natural to consider event shape measures in a first step and a further purification should be possible based on an analysis of the jet activity which is expected to be larger in top events.

The starting point is, as before, the general requirements in eq. (12) and also eqs. (9) and (10) when applicable. The cut in $\sum E_\perp$ is, however, increased to 40 GeV to achieve a stronger background suppression. This has a smaller effect on the signal, compared to the leptonic analysis, since there is in this case no large missing transverse energy from neutrinos in the top decay.

From the large energy available in the top quark decay one expects top events to be more spherical than background events. The usual sphericity measure, used in e^+e^- annihilation, is not suitable for ep collider events due to the presence of the target remnant jet. The latter can, however, be suppressed by applying the sphericity analysis in the transverse plane only. This transverse sphericity is then rather a measure of 'circularity' which can be defined by $C = 2\lambda_2$ in terms of the smaller eigenvalue, λ_2, of the two-dimensional sphericity tensor ($S_{\alpha\beta} = \sum_i p_{i\alpha}p_{i\beta}/\sum_i p_i^2$ where α, β are the transverse Cartesian components and i runs over the particles in the event). The resulting distributions in circularity for top events and the backgrounds are shown in Fig. 15. As discussed in [7], it is important to have as large a cut in $\sum E_\perp$ as possible to obtain the strong peaking of the backgrounds at small circularity in Fig. 15. This is another reason for the increase of the $\sum E_\perp$ cut to 40 GeV. With a cut in circularity of $C > 0.25$ the background is reduced by approximately a factor 10, while about one third of the signal is lost. With a much harder cut in $\sum E_\perp$, e.g. at 100 GeV, the backgrounds can be reduced below the top signal [7], but only at the expense of an undesirably large loss of top events.

The non-leptonic decay of a top quark is expected to produce three jets

$$t \to b + q + \bar{q} \to \text{jet} + \text{jet} + \text{jet} \tag{16}$$

In $\bar{t}b$ events one could therefore expect four jets in total and in $t\bar{t}$ events six jets. The number of observed jets may, however, be different depending on the jet reconstruction method and experimental limitations. Using the UA1-type algorithm described above, the jet multiplicity distributions in Fig. 16 are obtained. Typically, one or two jets less than expected are found in the top events, giving in the mean 3.0 (4.2) jets per $\bar{t}b$ ($t\bar{t}$) event ($m_t = 60$ GeV). In the background processes the jet multiplicity is determined by the amount of hard gluon radiation, which should ideally be calculated with exact matrix elements. Such are, however, presently limited to the lowest orders. Already the $O(\alpha_s^2)$ matrix elements are only available for some processes [19], and therefore a final state with at most three partons, or jets, can be described. Hence, these processes could be totally suppressed by a requirement of at least four jets. This would be unrealistically simple and it is therefore better to use the parton cascade approach, discussed above, to generate multijet final states. One has to keep in mind, however, the uncertainties in such models. The virtuality scale of the shower is not well-defined and the leading logarithm approximation employed is not designed for hard parton emission at wide angles, which is needed to produce separated jets. A factor ~ 2 uncertainty in the rate for each such emission is therefore possible. In a multijet rate this uncertainty is 'multiplied' and therefore increases powerlike with the number of hard branchings. The rate of background events with many jets, given in Fig. 16, must therefore be used with some caution.

From Fig. 16 it is clear that only a requirement of a rather large jet multiplicity can suppress the background substantially. The lower jet multiplicity in $\bar{t}b$ events means that they cannot be as efficiently selected as the $t\bar{t}$ events. At this point it is therefore advantagous

to divide the analysis in two lines, one being optimized for the $\bar{t}b$ events and the other for $t\bar{t}$ events. The selection procedures common for both cases are summarized in Tables 5 and 6, were the resulting cross-sections and mean values of the most important observables are given. Although no isolated lepton is present in these event samples there is still a substantial probability for a lepton to occur, in particular through the sequential bottom and charm decays in top events. Since these emerge within hadronic activity the identifiaction would only be straight-forward for muons. The last column in Table 6 shows the $p_\perp$ scale of these muons and indicates a possibility to make an additional selection hereby, although we have not persued this.

4.1 $\bar{t}b$-optimized analysis

Here we first require $n_{jet} \geq 3$ to improve the signal-to-background ratio, but still keep most of the $\bar{t}b$ statistics. The purity of the $\bar{t}b$ sample can then be improved by making use of the fact that this is a CC process which typically has a large $\not{p}_\perp$ from the scattered lepton, see eq. (11). The NC background should dominantly be at low $\not{p}_\perp$ and $t\bar{t}$ events are also not expected to have large $\not{p}_\perp$ when no isolated lepton is present. These expectations are borne out in Fig. 17, where the cross-section is given as a function of a cut in minimum $\not{p}_\perp$. With a requirement of $\not{p}_\perp > 15$ GeV all NC processes will be effectively suppressed ($t\bar{t}$ also, provided $m_t \geq 60$ GeV), with a very limited loss of the $\bar{t}b$ signal. However, the CC deep inelastic scattering, which has a large $\not{p}_\perp$ from the scattered lepton, is still considerably above the signal.

In summary, the cuts specifically designed to extract non-leptonic $\bar{t}b$ events are:

$$\sum E_\perp > 40\ GeV\ ,\ \ C > 0.25\ ,\ \ n_{jets} \geq 3\ ,\ \ \not{p}_\perp \geq 15\ GeV \qquad (17)$$

It is furthermore demanded that there is no isolated lepton as defined by eq. (14). For a 60 GeV top quark this gives a remaining $\bar{t}b$ ($t\bar{t}$) cross-section of 30 (7.5) fb while the total background is about a factor 20 larger. One could think of improving the signal-to-background ratio by requiring a larger jet multiplicity. With $n_{jet} \geq 4$, we find that all curves in Fig. 17 basically keep their shape but are scaled such that the signal-to-background is improved by a factor two, but at the prize of reducing the absolute rate in the signal by a factor three.

For this $\bar{t}b$ enriched sample one can now make use of the knowledge from the Monte Carlo concerning the origin of the reconstructed jets to optimize a top reconstruction procedure. As seen in Fig. 16, the $\bar{t}b$ sample is dominated by three and four jet events. In 3-jet events, the jets are mostly coming from the top quark decay, since the bottom quark is often not energetic enough to produce a reconstructable jet. A 4-jet final state is divided into three jets from the top decay and the forth identified with the bottom quark. In the latter case all combinations have to be considered since it is not obvious which jet is the b-quark one. We have tried topological signals to identify the b-quark jet, but not found any useful procedure. A tag of the bottom hadron or a vertex detector could be of great help, but are experimentally very involved issues which we have not investigated. Higher jet multiplicities are very rare and are therefore neglected when giving the invariant mass of various 3-jet combinations in Fig. 18. In the case of 4-jet events in Fig. 18b, the right and wrong combinations (given by the Monte Carlo) are shown separately for the $\bar{t}b$ events. The mass of the 3-jet system in 3-jet

$\bar{t}b$ events peaks nicely around the input top mass of 60 GeV, as do the right combinations of three out of four jets, Fig. 18a and 18b respectively. In the latter case, the peak barely stand out from the combinatorial background within the $\bar{t}b$ events themselves. The main background from normal deep inelastic charged current events (denoted by CC(e^-, W^2) in Fig. 18) is, however, considerably larger than these mass peaks, both in the case of 3 and 4 jets in the final state. Of course, the signal-to-background can be improved by integrating over a window in 3-jet mass around a top mass value which has been guessed based on other considerations. Cross-sections, for jet-combinations rather than events, obtained in such a way are examplified in Table 7.

The cross-section of the CC background is considerably larger than the $\bar{t}b$ signal. We emphasize, however, that HERA offers a 'trick' to reduce this background by using a positron beam instead of an electron one. Through the CC interaction a positron probes different quarks in the proton leading to a smaller total DIS cross-section. In fact the ratio $\sigma(e^+)/\sigma(e^-)$ decreases with increasing Q^2 which will make the cut in $\not{p}_\perp$ more effective. As shown in Fig. 18, the CC background in the top mass region is considerably lower in the e^+ case (denoted by CC(e^+, W^2)); approximately a factor 3.5 (5) for the case with 3 (4) jets in the final state. With this strong reduction of the background it may be possible to achieve a top reconstruction, in particular when integrating over a window in the 3-jet mass (cf. Table 7).

As discussed above, the background of multijet events arising from gluon emission is not well controlled in the parton cascade model and may well be overestimated. We note that more gluon radiation not only gives higher jet multiplicities but also a larger circularity and higher $\sum E_\perp$. These effects will all help in passing our cuts resulting in a possibly strong effect on the final sample. From this point of view it is very important to compare the parton shower results with exact matrix elements to the highest possible order. We note that parton shower models have been quite well tuned to data and order α_s^2 matrix elements in e^+e^- annihilation, but such studies remain to be performed in deep inelastic scattering. There are also enough theoretical differences between the two cases that the models cannot trivially be taken over from e^+e^- [14,20]. At present there is, therefore, a larger uncertainty in the DIS case. This is illustrated in Fig. 18 by showing the resulting CC background with a positron beam using two alternative scales for the parton cascade. With Q^2 as scale, instead of the prefered choice W^2 [14], a smaller background is obtained such that a signal-to-background ratio of about 0.5 (2) is obtained in the top mass region for the 3 (4) jet case. If this background estimate will prove more correct a quite decent result is thus obtained. Otherwise additional, or alternative, cuts have to be considered in order for this reconstruction method to give a clean enough top sample.

One such possibility [21] may be the invariant mass, W_{vis}, of the total observable hadronic system, i.e. outside the beam pipe, since for top events it should contain the threshold from the top quark mass. The invariant mass $\sqrt{\hat{s}}$ of the heavy $Q\bar{Q}$ system would be better to use, see [7], but is quite difficult to reconstruct experimentally. The extent to which W_{vis} differs from $\sqrt{\hat{s}}$ depends on how much of the target remnant jet is observed and thereby included in W_{vis}. Nevertheless, as shown in Fig. 19, the $\bar{t}b$ events and the CC background do have W_{vis}-distributions of different shapes *before* all other cuts have been applied. However, W_{vis} is correlated with the hadronic activity and therefore cuts in jet multiplicity and circularity provide implicit cuts in W_{vis}. In particular, low W_{vis} events are effectively suppressed. Thus

we find that by selecting a window in W_{vis} around the $\bar{t}b$ peak in Fig. 19 improves the signal-to-background ratio only marginally in the mass region of interest around the signal peak in Fig. 18, but it does lower the absolute rate in the $n_{jets} = 4$ case.

We have furthermore observed that the CC background and the top signal event samples, remaining at the end of our selection procedure, have rather similar distributions in most kinematical variables. There is, however, a clear difference in the Q^2 distributions, with $\bar{t}b$ events typically at lower values. The cuts in eq. (17) tend to favour large Q^2 values more strongly in the case of the CC background, whereas top events will also be favoured by the top decay dynamics. To resemble the experimental situation we apply a cut on the reconstructed value of Q^2 obtained through the standard 'Jacquet-Blondel' (see second paper in [14] and references therein). The cut $Q^2 < 1600$ GeV^2 reduces the $\bar{t}b$ sample to about one half, but it improves the signal-to-background ratio significantly. In the region of the top mass peaks in Fig. 18, this ratio is now found to be 1/4 (2/3) for an electron (positron) beam in the $n_{jets} = 3$ case and 1/2 (1/1) in case of $n_{jets} = 4$. Although the background is still not smaller than the signal, it has been reduced to a similar magnitude.

The differences between the top and background in terms of the other kinematical variables, i.e. x, y, Q^2 and W, are not large enough to give significant improvements by simple cuts. We note, however, that x-values lower than 0.01 do not occur at any appreciable rate. This means that there is no essential uncertainty in the background estimate due to uncertainties in the structure function parametrizations used. Furthermore, the typical Q^2 value (after all cuts) is not very much smaller than W^2, which is the reason why the use of these different scales for the parton cascade only give the limited uncertainty mentioned above and shown in Fig. 18.

One might expect that the $\bar{t}b$ events have a different topology compared to the CC background. The missing transverse momentum vector could, e.g., be more isolated in the latter case compared to the $\bar{t}b$ events where the top decay products are conceivably distributed more evenly in azimuthal angle. An inspection of visual event displays indicates that the background events are less likely to have a jet in the hemisphere of the $\not{p}_\perp$-vector. To investigate these possibilities we let this vector define zero azimuthal angle, i.e. $\Phi = 0$. The requirement of at least one jet within $|\Phi| < 90°$ is then found to improve the signal-to-background by about a factor 1.8, with only a 30% loss of the signal. This azimuthal asymmetry can also be quantified by the transverse energy in the same ($|\Phi| < 90°$) and opposite ($|\Phi| > 90°$) hemisphere as the $\not{p}_\perp$-vector, i.e.

$$A = \frac{E_\perp(|\Phi| > 90°) - E_\perp(|\Phi| < 90°)}{E_\perp(|\Phi| > 90°) + E_\perp(|\Phi| < 90°)} \tag{18}$$

The distributions in this observable are somewhat different for the $\bar{t}b$ signal and the CC background such that an improved selection can be obtained, e.g. the cut $A < 0.75$ increases the signal-to-background ratio by a factor 1.8 with a 22% loss of the signal.

This azimuthal asymmetry could also be reflected in event shape measures. We note, however, that both sphericity and thrust do not distinguish between these two hemispheres and are therefore not suitable. Instead we introduce a modified transverse thrust variable

$$\mathcal{T} = \frac{\sum_i \vec{n} \cdot \vec{p}_{\perp i}}{\sum_i |\vec{p}_{\perp i}|}, \quad \vec{n} = \frac{\vec{\not{p}}_\perp}{|\vec{\not{p}}_\perp|}. \tag{19}$$

The CC background, with a larger energy flow opposite to the $\not{p}_\perp$-vector, tend to have larger negative values of this observable. A cut $\mathcal{T} > -0.4$ is found to improve the signal-to-background ratio by about a factor 2.5 at the expense of a 55% loss of the $\bar{t}b$ signal. Due to the limited $\bar{t}b$ rate a milder cut is probably necessary, e.g. $\mathcal{T} > -0.5$ (-0.6) reduces the signal by 39% (16%) but still improves signal-to-background by a factor 2.2 (1.7).

From these examples of more involved topological cuts it is clear that an improved selection of non-leptonic $\bar{t}b$ events can be achieved. There are, however, no strong differences in the characteristics of the signal and background events and one can therefore not gain large factors in the signal-to-background ratio without a substantial loss of the absolute rates. Nevertheless, a factor 2–3 improvement with only a limited loss of the signal should be possible if cuts of this kind are combined and fine-tuned. In the case of a positron beam this would bring the background down to the same level as the top signal and hence a peak in the 3-jet mass spectrum (Fig. 18) should emerge for the case $m_t = 60$ GeV.

The results in terms of cross-sections, mean values and mass reconstruction for the non-leptonic $\bar{t}b$ anaysis are summarized in Table 5–7. As mentioned, the dominant CC background may be overestimated through the use of the parton cascade scheme to generate multijet events. If so, the top mass recontruction will be correspondingly better and may well extend to about 70 GeV. The electron beam option could then also give useful results in this respect. Otherwise, a positron beam is strongly favoured and we have shown the possibility to reconstruct the mass of a 60 GeV top quark using detailed topology requirements in terms of jets and, e.g., energy flow asymmetries or a new thrust variable. In case of a heavier top quark the reconstruction method would give essentially the same signal-to-background ratio, only the the absolute rates will decrease, e.g. by about a factor three for $m_t = 80$ GeV. Thus, the limit is given by statistics and not the analysis procedure.

Finally, we note that if it would be possible to tag bottom particles completely new perspectives would open, e.g. the dominating CC background could be more efficiently rejected and a cleaner $\bar{t}b$ sample obtained. The possibility to observe secondary vertices using a vertex detector would also provide new ways to select heavy flavour events and thus reject other types of background processes. In view of the small top event statistics, however, both these methods must be quite efficient to be of any use for a top search. To evaluate this would require very detailed experimental considerations which are beyond the scope of the present study.

4.2 $t\bar{t}$-optimized analysis

We now turn to an analysis dedicated to the non-leptonic $t\bar{t}$ sample. As argued earlier in connection with Fig. 3, one can here require a larger $\sum E_\perp$ without loss of signal and we thus select events with $\sum E_\perp > 80$ GeV. A larger jet multiplicity can also be used to obtain a purer $t\bar{t}$ sample, as seen from Fig. 16. (The jets are defined by the UA1-type of jet algorithm as discussed above.) The requirement $n_{jets} \geq 4$, which gives a substantial improvement in the signal-to-background ratio without too serious loss of $t\bar{t}$ events, will be primarily used. As an alternative we also try the stronger cut $n_{jets} \geq 5$ to find the practical limit in terms of

remaining statistics. The selection criteria to obtained a sample enriched in non-leptonic $t\bar{t}$ events are then:

$$\sum E_\perp > 80\ GeV\ ,\ \ C > 0.25\ ,\ \ n_{jets} \geq 4\ \ \{\text{or, alternatively } 5\}\ . \qquad (20)$$

together with the requirement that there is no isolated lepton as defined by eq. (14). Resulting cross-sections for signal and backgrounds are summarized in Table 5, and also in Table 8. The background, which is dominated by the NC process $\gamma + q \rightarrow q + g$ at low Q^2, has a larger cross-section than the $t\bar{t}$ signal.

The $t\bar{t}$ signal may still be larger in a limited region of some differential distribution. For this reason and in order to attempt a measurement of the top quark mass through a mass peak reconstruction we proceed similarly to the isolated-lepton analysis for the $t\bar{t}$ case in section 3.2. The obtained event samples are thus subjected to the second jet finding algorithm, described above, where the number of jets are now forced to be six. This corresponds to the expectation of three jets in the non-leptonic decays of both the t and $\bar{t}$ quark. The invariant mass of 3-jet combinations can now be formed and the resulting distributions are shown in Fig. 20. As for the previous cases, there is a problem of combinatorics which is here accentuated since a 3-jet combination can be selected in 20 different ways from an event containing six jets. This has the effect that already in the top events themselves the many wrong ($t\bar{t}_W$) combinations overwhelms the right ($t\bar{t}_R$) combinations (right and wrong is given by the knowledge available in the Monte Carlo generator). The major background is, however, given by NC processes at low Q^2. The dominating contribution is $\gamma + q \rightarrow q + g$, but also $\gamma + g \rightarrow q + \bar{q}$ is important; in both cases with additional parton emission as discussed in section 2. The charged current DIS process gives a smaller background which, however, also can mask the signal. As noted above, this process can be greatly reduced, as shown in Fig. 20a, by the use of a positron beam. The higher jet multiplicity requirement in this $t\bar{t}$ analysis, as compared to the non-leptonic $\bar{t}b$ case above, implies not only a more effective background suppression, but also a stronger sensitivity to the mentioned uncertainties in the parton cascade. At least 2 (3) hard branchings are necessary to obtain the required minimum of 4 (5) jets in Fig. 20a (b). To illustrate this uncertainty we show the resulting CC background in the e^+p case for two alternative parton cascade scales in Fig. 20a.

In the same way as discussed for the semi-leptonic $t\bar{t}$ case (see Fig. 13) one can select a window in the two-dimensional distribution $d^2\sigma/dm(j_1j_2j_3)dm(j_4j_5j_6)$. This is demonstrated in Fig. 21, where only the right jet combinations are seen to peak at the proper place, i.e. $m(j_1j_2j_3) = m(j_4j_5j_6) = m_t$, whereas all wrong combinations in both background and top events have a rather flat distribution. By using only those jet combinations where *both* 3-jet masses fall in the range [57,63] GeV, around the peak in Fig. 21d, a very strong suppression of the background and the wrong jet combinations is obtained. In the resulting 3-jet mass distributions, Fig. 22, the right combinations now peaks above the wrong ones in $t\bar{t}$ events. The dominating NC background has been reduced to the same magnitude as the signal in the $n_{jets} \geq 4$ case and significantly below it for $n_{jets} \geq 5$, Fig. 22 a and b respectively. The observable distribution, which is the sum of all curves, will therefore show a tendency of a bump already in the former case and a more clear peak in the latter. If the jet multiplicity in the DIS background is indeed overestimated, as discussed above, an even more favourable situation would arise. The relevant cross-sections and number of events are summarized in Table 8. (Cross-sections are for jet combinations and do therefore not exactly correspond

to the number of events.) In the $n_{jets} \geq 5$ case, for example, the total cross-section in the 3-jet mass region [57,63] GeV is 7.5 fb with 3.8 fb given by the correct jet combinations in $t\bar{t}$ events.

The large combinatorial background resulting from the 6-jet final state would of course have been smaller if the 3-jet mass combinations were formed from the original 4 or 5 jets dominating the two samples. However, without the forced 6-jet final states the window in the two-dimensional distribution could not have been formed and this trick to reduce the background not been employed. The background, corresponding to that in Fig. 20, is therefore found to be above the signal also in such an analysis. With the loss of jets the mass peaks will also be broader and need not peak at the input top quark mass. In fact, it is a non-trivial result that we obtain mass peaks at the proper place when reconstructing a predefined number of jets corresponding to the expected jet multiplicity in the relevant top sample.

The analysis designed for the non-leptonic $t\bar{t}$ sample is summarized in the following tables: cross-sections in Table 5, mean values of some important observables in Table 6 and the top mass reconstruction in Table 8. The high jet multiplicity in $t\bar{t}$ is an advantage with respect to the background, but leads to an accentuated problem of combinatorics when searching for a peak in the invariant mass of jet combinations. Nevertheless, the background can be suppressed to the same level as the top signal for events with at least 4 jets, and even below the signal when 5 jets are required. The remaining event rate is, however, very small and long running periods are therefore necessary. A top mass of 60 GeV is still possible to reconstruct, but with higher mass too few events are expected to allow a mass measurement, although single top candidate events may still be observed.

5 Discussion

Searching for the top quark is a major challange at every new accelerator giving access to higher energies in different kinds of interactions. In this paper we have performed the first detailed study of top search strategies in ep collisions at the HERA energy. The selection criteria and analysis procedures developed are based on measurable observables and therefore experimentally realistic results are presented. This was achieved by investigating both the top production as well as all relevant background processes using Monte Carlo simulation techniques that produce complete events. Higher order parton emission processes are here included as well as hadronization and heavy flavour decays.

Top quark production at the HERA energy is expected to be dominated by the process of boson-gluon fusion, which occurs in first order QCD. In neutral current interactions a $t\bar{t}$ pair is produced, whereas the charged current process gives rise to a $\bar{t}b$ pair. The latter process dominates if the top quark mass is larger than about 55 GeV, due to the lower threshold for single top production as compared to pair production. Given the present top quark mass limits of about 50 GeV, the production cross-section is unfortunately small and decreases rapidly with increasing mass. The statistical limitations with only a few events in the remaining samples, after cuts to reduce the background, will therefore be a severe problem. We note, however, that the numbers given above are rather on the low side since

the we use a mass scale for α_s and the gluon density which is the largest realistic one. As discussed in section 2, the smallest such scale leads to a factor two larger top cross-section. It is therefore important to calculate the full next-to-leading order corrections in order to minimize this theoretical uncertainty.

As backgrounds we have considered hard scattering processes at low Q^2, i.e. photoproduction, and the deep inelastic processes. Neither of them can *a priori* be neglected. Depending on the signatures used for the top search, one or the other will be most difficult to suppress to a level comparable with, or below, the top signal.

Different main roads of top searches have been tried, e.g. based on lepton or multijet signatures, and several observables been investigated in detail to find suitable cuts and selection criteria. We do not claim to have found the best possible strategies but, given the many detailed analyses, we think that the procedures developed are not far from being optimal. It should be noted that a possibility to tag bottom particles would lead to an improved analysis. Likewise, the observation of secondary vertices through a high resolution vertex detector would enable the selection of heavy flavour events and hence rejection of other backgrounds. Although such additional information could improve a top search significantly, it is clear that the small top event statistics would require a high efficiency for these methods to be useful. An evaluation of this would involve a detailed consideration of several experimental problems. This is beyond the scope of this paper and it is therefore not possible at present to base a realistic study on such methods.

Signatures based on the semileptonic top decays were examined in two major ways. The requirement of two leptons in an event provides a quite useful signature in case of a rather light top quark. For a mass above 50–60 GeV, however, the signal-to-background ratio is too small to be of practical use. On the other hand, a single lepton which is isolated from other particles gives a very useful signature. Together with cuts on total transverse energy and missing transverse momentum, this can give a non-vanising top sample, which is free from backgrounds, also in case of a heavier top quark. For example, with $m_t = 80$ GeV we expect 2 events for an integrated luminosity of 200 pb^{-1} obtainable in a full year of HERA running. The number of events with this isolated lepton signature will give a good estimate for the top quark mass, but a proper measurement through a peak in suitable invariant masses is more demanding and can only be made for $t\bar{t}$ events where only one high energy neutrino is present. We have demonstrated that such a measurement is possible for a 60 GeV top quark mass where 2 events per 200 pb^{-1} are expected. Although this is a small number, each $t\bar{t}$ event gives two mass estimates, namely from the semileptonic and the hadronic decay, respectively. We emphazise that we have obtained a unique top signature without any surviving background events. Of course, with some years of data taking the sample will also increase and give a correspondingly improved result. The practical limit for this mass reconstruction seems to be around $m_t = 70$ GeV at which point only 2 events per four years are expected in the final mass peak.

The larger branching ratio of non-leptonic top decays can be exploited by a selection procedure based on requirements on the total transverse energy, event shape and jet multiplicity. These signatures are, however, not specific enough for top events to provide cuts that suppress all background processes to a negligible level. The remaining background is furthermore somewhat uncertain in magnitude since it depends on the details concerning the event shape

and, in particular, the probability of multijet final states. Higher order QCD processes are here of importance, but have not yet been calculated exactly. A leading logarithm parton cascade treatment of multiple parton emission was therefore used. The uncertainty in this framework is hence inherent in our results and we stress the importance of future work to check the reliability of this scheme in comparison with exact QCD matrix elements of highest possible order.

When selecting preferentially $\bar{t}b$ events from e^-p interactions, the dominating charged current background (involving light quarks) is considerably larger than the signal. Using a positron beam, however, this is reduced to a level comparable to the top signal. By applying additional, but rather detailed, topology cuts it is possible to improve the signal-to-background by a factor 2–3 with a rather limited loss of the absolute top rate. This may not be sufficient for a mass reconstruction in e^-p interactions, but for the e^+p case a mass peak above the background should be possible for a 60 GeV top quark. The $\bar{t}b$ sample has also the potential of at least giving top candidate events up to $m_t = 80$ GeV, although a proper mass measurement is probably limited to about 70 GeV for statistical reasons.

A non-leptonic $t\bar{t}$ analysis can provide a peak above background in the distribution of the invariant mass of three-jet combinations and hence provide a top quark mass measurement. This is, however, in practice limited to about 60 GeV since the absolute rate would be too small for a higher mass.

These positive results were, however, only possible through the analysis procedures developed in this work. In particular, the following 'tricks' proved very useful. In order to reconstruct the top quark mass through the invariant mass of combinations of jets (and leptons) we forced the number of reconstructed jets to be that expected from the top decay topology. Background events as well as wrong jet combinations in $t\bar{t}$ events were then strongly suppressed by requiring the mass of the two complementary combinations in the same event to fall in a window around the expected top quark mass or, alternatively, selecting only that combination of jets which gives the smallest mass difference. In addition some new topological measures, like an energy flow asymmetry and a modified thrust variable, were introduced.

The event samples used in the two main parts of our study, the semi-leptonic and the non-leptonic analyses, are complementary with no events in common. The top event samples obtained from these two cases can therefore be added to obtain a larger total statistics of top events. The resulting precision of the top mass measurements will also be correspondingly better. For small top event samples this will, of course, be of particular importance.

As expected in the introduction, we have found that the background problems are indeed less severe in ep collisions as compared to the situation in $p\bar{p}$ interactions. Our signature based on an isolated lepton can give a unique selection of top events without any remaining background, whereas in $p\bar{p}$ this does not seem to be the case. Searches based on the non-leptonic decay mode of the top quark are very difficult in $p\bar{p}$, but can give useful results in the ep case. We therefore conclude that ep interactions do indeed provide a competitive alternative for hunting the top quark. Thus, HERA may have a chance to actually discover a top quark in the mass range 50 to 80 GeV. In case of a larger top quark mass, ep collisions in a possible future combinations of LEP and LHC would of course be of interest.

The major limitation for HERA is given by statistics, in particular since one cannot avoid loosing top events when applying cuts to suppress the backgrounds. The remaining signal

is therefore always very small in absolute terms and a strong effort must be made to obtain as large integrated luminosity as possible. Besides long running times, any increase in the luminosity is most wellcome. We also note that the charged current $\bar{t}b$ cross-section can be increased with a polarized beam; the gain being a factor $1 \mp \lambda$ for electron (positron) polarization λ ($= \pm 1$ for a right/left-handed state). In the background free isolated-lepton sample this factor has an immediate effect. In the non-leptonic sample the signal-to-background ratio stays constant, but the absolute level of the signal would improve by this factor. Finally, we emphazise that with the HERA energy, top production is still close to threshold. Any increase of the beam energies will therefore have a significant effect on the top cross-section [7]. For example, 35 GeV electrons on 1000 GeV protons would give a factor 2–3 increase of the production rate, for m_t =50–100 GeV, and is therefore equivalent to a non-trivial increase of luminosity or running time.

Acknowledgements. We are very grateful to Dr. F. Barreiro for interesting and helpful discussions as well as contributions to an early phase of this analysis. Useful discussions with Dr. E. Gotsman are also acknowledged.

References

[1] C. Albajar et al., UA1 collaboration, Z. Phys. C37 (1988) 505

[2] H. Albrecht et al., ARGUS collaboration, Phys. Lett. 192B (1987) 245

[3] W. Bartel et al., JADE Collaboration, Phys. Lett. 129B (1983) 145; ibid. 160B (1985) 337
M. Althoff et al., TASSO Collaboration, Phys. Lett. 138B (1984) 441; ibid. 154B (1985) 236
H.J. Behrend et al., CELLO Collaboration, Phys. Lett. 144B (1984) 297
B. Adeva et al., MARK-J Collaboration, Phys. Lett. 152B (1985) 439

[4] H. Yoshida et al., VENUS Collaboration, Phys. Lett. 198B (1987) 570
H. Sagawa et al., AMY Collaboration, Phys. Rev. Lett. 60 (1988) 93
I. Adachi et al., TOPAZ Collaboration, Phys. Rev. Lett. 60 (1988) 97

[5] G.A. Schuler, Nucl. Phys. B299 (1988) 21

[6] M. Glück, R.M. Godbole, E. Reya, Z. Phys. C38 (1988) 441
U. Baur, J.J. van der Bij, Nucl. Phys. B304 (1988) 451
R.A. Eichler, Z. Kunszt, ETHZ-IMP-P/88-1

[7] G. Ingelman, G.A. Schuler, Z. Phys. C40 (1988) 299

[8] G. Ingelman, G.A. Schuler, AROMA 1.2 – A Generator of Heavy Flavour Events in *ep* Collisions, DESY preprint in preparation

[9] E. Eichten, I. Hinchliffe, K. Lane, C. Quigg, Rev. Mod. Phys. 56 (1984) 579, ibid. 58 (1986) 1047

[10] T. Sjöstrand, M. Bengtsson, Comput. Phys. Common. 43 (1987) 367

[11] B. Andersson, G. Gustafson, G. Ingelman, T. Sjöstrand, Phys. Rep. 97 (1983) 31

[12] R.P. Feynman, Photon-hadron interactions, W.A. Benjamin Inc. 1972.

[13] G. Ingelman, LEPTO 5.2, DESY preprint in preparation

[14] M. Bengtsson, T. Sjöstrand, Z. Phys. C37 (1988) 465
M. Bengtsson, G. Ingelman, T. Sjöstrand, Nucl. Phys. B301 (1988) 554

[15] B. Andersson, G. Gustafson, G. Ingelman, T. Sjöstrand, Z. Phys. C13 (1982) 361

[16] G. Ingelman, D. Notz, E. Ros, Proc. workshop on 'Physics at HERA', Hamburg, October 1987, Ed. R.D. Peccei, vol. I, p. 19

[17] V. Barger, A.D. Martin, R.J.N. Phillips, Phys. Lett. 125B (1983) 339, 343; Phys. Rev. D28 (1983) 145
E.L. Berger, D. Dibitonto, M. Jacob, W.J. Stirling, Phys. Lett. 140B (1984) 259

[18] T. Sjöstrand, Computer Phys. Comm. 28 (1983) 229

[19] R.K. Ellis, Z. Kunszt, Nucl. Phys. B303 (1988) 653
R.K. Ellis, P.Nason, FERMINLAB-Pub-88/54-T

[20] J.G. Körner, E. Mirkes, G.A. Schuler, DESY 88-095

[21] H.R. Wilson, Cavendish-HEP-88/3

Table 1

Characteristics of heavy quark and background events

Cuts: beam hole angle $\theta = 100$ mrad

for DIS: $Q^2 > 4\ GeV^2$, $x > 10^{-3}$, $W^2 > 5\ GeV^2$

for light quark events: $p_\perp \geq 1$ GeV

process	σ[pb]	$\langle \sum E_\perp \rangle$[GeV]	$\langle C \rangle$	$\langle n_{ch} \rangle$
NC				
$b\bar{b}$	4.2×10^3	14.	0.44	16
$c\bar{c}$	5.1×10^5	7.2	0.51	12
DIS	1.3×10^5	8.6	0.12	5
qG	7.3×10^5	3.4	0.42	5
$q\bar{q}$	7.8×10^5	6.2	0.50	10
CC				
$\bar{c}s$	8.3	25.	0.18	13
light quarks	71.	42.	0.14	15
$\bar{t}b$ $m_t =$				
40 GeV	0.36	48.	0.30	21
60 GeV	0.13	58.	0.28	21
80 GeV	0.05	70.	0.26	22
$t\bar{t}$ $m_t =$				
40 GeV	1.9	66.	0.36	26
60 GeV	0.09	93.	0.37	28
80 GeV	4.3×10^{-3}	117.	0.38	29

Table 2

Dilepton events: cross sections and mean lepton $p_\perp$					
General cuts: eq. (12) and $\sum E_\perp > 40$ GeV eqs. (9) and (10) when applicable					
Cuts					
$p_\perp(l_1)$ [GeV] $\geq$	0	0	10.	10.	10.
$p_\perp(l_2)$ [GeV] $\geq$	0	0	0	0	5.
Process	σ[pb]	$\langle p_\perp(l_1)\rangle$ [GeV]	σ[fb]	$\langle p_\perp(l_2)\rangle$ [GeV]	σ[fb]
NC					
$b\bar{b}$	3.4	4.2	350.	3.1	73.
$c\bar{c}$	9.5	1.8	110.	3.2	28.
DIS	–	–	–	–	–
qG	12.	0.62	1.7	4.5	0.52
$q\bar{q}$	6.2	0.61	0.32	3.1	0.07
CC					
$\bar{c}s$	0.14	1.2	1.6	1.5	0.17
light quarks	2.4	1.1	31.	4.1	12.
$\bar{t}b$ $m_t =$					
40 GeV	0.096	6.5	22.	3.4	5.1
60 GeV	0.046	8.6	15.	3.5	3.6
80 GeV	0.019	10.	7.2	3.8	1.9
$t\bar{t}$ $m_t =$					
40 GeV	0.79	8.6	270.	4.5	92.
60 GeV	0.038	12.	19.	5.7	8.2
80 GeV	0.002	15.	1.1	6.8	0.52

Table 3

Cross-sections [fb] for events containing a lepton					
General cuts: eq. (12), also eqs. (9) and (10) when applicable					
Process	total	$p_\perp^l \geq 8$ GeV	$E_{acc} \leq 1$ GeV	$\not{p}_\perp \geq 10$ GeV	$\sum E_\perp \geq 60$ GeV
$b\bar{b}$	2.7×10^5	3.2×10^3	7.5×10^2	1.1†	0.01†
$c\bar{c}$	1.1×10^6	1.4×10^3	5.2†	0.008†	0.008†
$\bar{c}s$	1.3×10^3	40.	0.	0.	0.
light quarks	2.3×10^4	10.	0.	0.	0.
$\bar{t}b$ $m_t =$					
40 GeV	0.28×10^3	71.	48.	40.	5.4
60 GeV	0.10×10^3	35.	25.	21.	5.0
80 GeV	38.	15.	9.9	8.9	3.6
$t\bar{t}$ $m_t =$					
40 GeV	1.3×10^3	0.49×10^3	0.37×10^3	0.22×10^3	96.
60 GeV	59.	29.	21.	16.	14.
80 GeV	2.7	1.6	1.0	0.9	0.9

† Based on few events in remaining Monte Carlo sample.

Table 4

Mean values [GeV] for events containing a lepton				
General cuts: eq. (12), also eqs. (9) and (10) when applicable				
Cuts:		$p_\perp^l \geq 8\,\text{GeV}$	$E_{acc} \leq 1\,\text{GeV}$	$\not{p}_\perp \geq 10\,\text{GeV}$
Process	$\langle p_\perp^l \rangle$	$\langle E_{acc} \rangle$	$\langle \not{p}_\perp \rangle$	$\langle \sum E_\perp \rangle$
$b\bar{b}$	2.0	1.9	2.1	31.†
$c\bar{c}$	1.1	3.1	1.6†	–‡
$\bar{c}s$	1.7	1.7	–	–
light quarks	0.6	$\geq 5.$	–	–
$\bar{t}b \quad m_t =$				
40 GeV	5.8	0.52	20.	44.
60 GeV	7.5	0.41	22.	50.
80 GeV	9.0	0.38	25.	58.
$t\bar{t} \quad m_t =$				
40 GeV	7.5	0.44	13.	60.
60 GeV	11.	0.42	19.	82.
80 GeV	13.	0.35	23.	104.

† Based on few events in remaining Monte Carlo sample.

‡ No event surviving the cuts.

Table 5

Cross-sections [fb] in non-leptonic analysis						
General cuts: eq. (12) and $\sum E_\perp > 40$ GeV eqs. (9) and (10) when applicable						
Cuts						
$C \geq$	0	0.25	0.25	0.25	0.25	0.25
$n_{jets} \geq$	0	0	3	3	4	4
$\not{p}_\perp$ [GeV] $\geq$	0	0	0	15.	0	0
$\sum E_\perp$[GeV] $\geq$	40	40	40	40	40	80.
Process						
NC						
$b\bar{b}$	$13. \times 10^3$	1.5×10^3	0.78×10^3	2.4	41.	8.7
$c\bar{c}$	$64. \times 10^3$	6.1×10^3	3.8×10^3	5.5	0.17×10^3	19.
DIS	2.9×10^3	–‡	–	–	–	–
low Q^2 qG	$90. \times 10^3$	$12. \times 10^3$	8.3×10^3	22.†	0.66×10^3	0.15×10^3
low Q^2 $q\bar{q}$	$51. \times 10^3$	4.4×10^3	2.8×10^3	–	0.17×10^3	15.
CC						
$\bar{c}s$	1.4×10^3	0.20×10^3	25.	21.	0.80	0.37
light quarks	$27. \times 10^3$	2.6×10^3	0.73×10^3	0.70×10^3	0.10×10^3	48.
$\bar{t}b \quad m_t =$						
40 GeV	0.22×10^3	0.14×10^3	81.	59.	17.	2.4
60 GeV	94.	54.	41.	30.	13.	4.7
80 GeV	37.	19.	16.	11.	5.2	3.8
$t\bar{t} \quad m_t =$						
40 GeV	1.1×10^3	0.77×10^3	0.68×10^3	92.	0.41×10^3	0.13×10^3
60 GeV	46.	34.	33.	7.5	26.	23.
80 GeV	2.1	1.5	1.5	0.42	1.3	1.3

† Based on few events in remaining Monte Carlo sample.

‡ No event surviving the cuts.

Table 6

Mean values in non-leptonic analysis					
General cuts: eq. (12) and $\sum E_\perp > 40$ GeV eqs. (9) and (10) when applicable					
Cuts					
$C \geq$	0	0.25	0.25	0.25	0.25
$n_{jets} \geq$	0	0	3	3	3
Process	$\langle C \rangle$	$\langle n_{jets} \rangle$	$\langle \sum E_\perp \rangle$ [GeV]	$\langle \not{p}_\perp \rangle$	$\langle p_\perp^\mu \rangle$
NC					
$b\bar{b}$	0.12	2.5	52.	2.1	0.96†
$c\bar{c}$	0.10	2.7	51.	1.4	0.36†
DIS	–‡	–	–	–	–
low Q^2 qG	0.13	2.7	56.	1.0†	–‡
low Q^2 $q\bar{q}$	0.096	2.7	53.	0.89†	–‡
CC					
$\bar{c}s$	0.11	2.1	59.	27.	0.18
light quarks	0.082	2.3	70.	34.	–
$\bar{t}b$ $m_t =$					
40 GeV	0.36	2.7	60.	23.	1.3
60 GeV	0.34	3.0	70.	23.	1.4
80 GeV	0.31	3.1	82.	23.	1.6
$t\bar{t}$ $m_t =$					
40 GeV	0.42	3.6	71.	6.6	1.8
60 GeV	0.42	4.2	99.	9.2	2.4
80 GeV	0.42	4.5	126.	11.	2.9

† Based on few events in remaining Monte Carlo sample.

‡ No event surviving the cuts.

Table 7

Top mass reconstruction designed for non-leptonic $\bar{t}b$ events					
General cuts: eq. (12) and $\sum E_\perp > 40$ GeV eqs. (9) and (10) when applicable no isolated lepton, circularity > 0.25, $\not{p}_\perp > 15$ GeV					
Cuts					
n_{jets}	≥ 3	≥ 4	$= 3$	$= 4$	$= 4$
m(3-jet) [GeV] $\in$	–	–	[50,62]	[50,62]	[50,62]
				sum of all 3-jet combinations	right 3-jet combination
Process	σ[fb]				
CC (e^-, W^2)†	750.	92.	147.	80.	–
CC (e^+, W^2)†	254.	21.	44.	14.	–
CC (e^+, Q^2)†	160.	7.7	28.	4.5	–
$\bar{t}b$	30.	8.9	11.	14.	6.2
$t\bar{t}$	7.5	4.3	0.8	4.8	–

† Charged current background for $e^\mp$ beam using W^2 or Q^2 as parton cascade scale.

Table 8

Top mass reconstruction designed for non-leptonic $t\bar{t}$ events			
General cuts: eq. (12) and $\sum E_\perp > 80$ GeV eqs. (9) and (10) when applicable no isolated lepton, circularity > 0.25 $n_{jets} \geq 4$ {or, alternatively 5} (UA1 algorithm) new jet reconstruction forces 6 jets			
Further cuts:	none	$m(j_1j_2j_3), m(j_4j_5j_6) \in [57,63]$ GeV	
		sum of all combinations	right jet combinations
Process	σ[fb]		
NC background	3.9×10^3 {0.60×10^3}	8.7 {1.†}	– {–}
CC background	960. {96.}	1.9† {–}	– {–}
$\bar{t}b$	94. {8.2}	0.14 {0.021}	– {–}
$t\bar{t}$	460. {260.}	9.5 {6.5}	5.2 {3.8}
Process	# events in 1 fb^{-1}		
NC background	220. {30.}	6.6 {0.77†}	– {–}
CC background	48. {4.8}	1.9† {–}	– {–}
$\bar{t}b$	4.7 {0.41}	0.12 {0.019}	– {–}
$t\bar{t}$	23. {13.}	7.8 {5.3}	5.2 {3.8}

† Based on few events in remaining Monte Carlo sample.

Figure captions

Figure 1 (a) Normal charged current interaction with flavour mixing giving a single heavy quark. (b) First order QCD diagrams for boson-gluon fusion into a heavy quark-antiquark pair.

Figure 2 Cross-section for top quark production via boson-gluon fusion as a function of the top quark mass. The curves are for $\bar{t}b$ production in charged current interactions (W), and for $t\bar{t}$ production in the neutral current case separately for pure γ, pure Z and their interference $\gamma - Z$. The inclusive cross-section is for $t + \bar{t}$ as defined in eq. (6).

Figure 3 Distribution in total transverse energy, $\sum E_\perp$ (based on stable particles outside a beam pipe cone of 5.7° and excluding the scattered $e^\mp$ in NC interactions), for $t\bar{t}$, $\bar{t}b$ events ($m_t = 60$ GeV) and the various background processes as discussed in the text.

Figure 4 Total cross-section of lepton pair production (excluding the scattered lepton) as function of a minimum lepton $p_\perp$. In (a) the cut is in the highest-$p_\perp$ lepton and in (b) in the second lepton $p_\perp$ after requiring the first lepton to have $p_\perp > 10$ GeV. The curves are NC charm plus bottom background (dotted), all other backgrounds without heavy quarks (dashed) and the total $t\bar{t}+ \bar{t}b$ signal (full) for three top quark masses. The events also fulfil $\sum E_\perp > 40$ GeV and eq. (12).

Figure 5 Cross-section for lepton ($\mu^\pm, e^\pm$) events as a function of a lower cutoff on the lepton transverse momentum w.r.t. to the beam axis. (The highest-$p_\perp$ lepton is taken in multilepton events.) The events also satisfy eq. (12).

Figure 6 Cross-section as a function of lepton isolation, defined by the maximum transverse energy E_{acc}^{cut} in a cone of size $\Delta R = 0.4$ (see eq. (13)) around a lepton with $p_\perp > 8$ GeV. The events also satisfy eq. (12).

Figure 7 Cross-section versus a minimum missing transverse momentum, $\not{p}_\perp{}^{cut}$, for events with an isolated lepton as defined by eq. (14). The curves are for CC and NC top production as well as for the remaining $b\bar{b}$ and $c\bar{c}$ backgrounds. The conditions in eq. (12) are also applied.

Figure 8 Total number of events, at an integrated luminosity of 1 fb^{-1}, in top signal plus backgrounds as a function of the top quark mass. The events have an isolated lepton, eq. (14), and fulfil the additional conditions indicated. The bands correspond to lower and upper limits at 68% CL, calculated with Poisson statistics from the cross-sections in Table 3. The background levels contain a 1σ increase to give the upper limit at 68% confidence level.

Figure 9 Differential cross-section in missing transverse momentum for events with an isolated lepton (defined by eq. (14)). The curves correspond to CC and NC production of top quarks of different indicated masses, and the remaining background ($b\bar{b}$). The conditions in eq. (12) are also applied.

Figure 10 Differential cross-section in total transverse energy for events with an isolated lepton (defined by eq. (14)) and with $\not{p}_\perp > 10$ GeV. Curves are for CC and NC production of top quarks of different indicated masses, as well as the remaining background ($b\bar{b}$). Conditions in eq. (12) are also imposed.

Figure 11 Distribution in the number of jets, reconstructed with a UA1-type algorithm, in events with an isolated lepton (defined by eq. (14)) and with $\not{p}_\perp > 10$ GeV. The curves correspond to $t\bar{t}$ and $\bar{t}b$ production, with $m_t = 60$ GeV, and the remaining background ($b\bar{b}$). Requirements in eq. (12) also satisfied.

Figure 12 Distributions in mass from combinations of reconstructed jets (j), the isolated lepton (l) and $\not{p}_\perp$ (ν) to obtain the top quark mass through its semileptonic and hadronic decays. (a) Minimum mass $m_l = m(l\nu j)$ and (b) invariant mass $m_h = m(jjj)$ of the three remaining jets. The curves correspond to right and wrong combinations in $t\bar{t}$ events and all combinations in $\bar{t}b$ events. The events contain an isolated lepton (defined by eq. (14)), have $\not{p}_\perp > 10$ GeV and $\sum E_\perp > 60$ GeV as well as at least three jets which are regrouped to exactly four jets.

Figure 13 Twice differential distribution, $d^2\sigma/dm_l dm_h$, in 'leptonic' and 'hadronic' masses for (a) background events, (b) $\bar{t}b$ events, (c) wrong and (d) right jet combinations in $t\bar{t}$ events. Conditions and notations as in Fig. 12.

Figure 14 As Fig. 12, but for each event only that combination of jets is taken which minimize $|m_l - m_h|$.

Figure 15 Differential cross-section in circularity for the total NC and CC backgrounds and the top signal, separately for $\bar{t}b$ and $t\bar{t}$ events. The events do not have an isolated lepton, are subject to the cuts in eq. (12) and have $\sum E_\perp > 40$ GeV.

Figure 16 Jet multiplicity distributions, obtained by a UA1 type algorithm, for the total NC and CC backgrounds as well as for the $\bar{t}b$ and $t\bar{t}$ signals ($m_t = 60$ GeV). The events, passing the cuts in eq. (12), do not have an isolated lepton, but have $\sum E_\perp > 40$ GeV and circularity $C > 0.25$.

Figure 17 Cross-section versus a minimum missing transverse momentum, $\not{p}_\perp{}^{\rm cut}$, for the total NC and CC backgrounds and the top signal events for different indicated top quark masses. The events satisfy the requirements: eq. (12), no isolated lepton, $\sum E_\perp > 40$ GeV, circularity $C > 0.25$ and $n_{jet} \geq 3$.

Figure 18 Distribution in the invariant mass of 3-jet combinations in (a) 3-jet events and (b) 4-jet events. In (b) the right ($\bar{t}b_R$) and wrong ($\bar{t}b_W$) combinations of $\bar{t}b$ events are shown separately, whereas all combinations are summed for $t\bar{t}$ and the background. The CC background curves are for electron and positron scattering using W^2 and Q^2 as the scale in the parton cascade. The events satisfy the requirements: eq. (12), no isolated lepton, $\sum E_\perp > 40$ GeV, circularity $C > 0.25$ and $\not{p}_\perp > 15$ GeV.

Figure 19 Distribution in the invariant mass W_{vis} of the complete *observable* hadronic system in $\bar{t}b$ events and total CC background (notation of curves as in Fig. 18). The events satisfy the requirements: eq. (12), no isolated lepton, $\sum E_\perp > 40$ GeV.

Figure 20 Distribution in the invariant mass of 3-jet combinations in non-leptonic events where 6-jet final states have been forced (by another jet finding algorithm) from events originally having (a) 4 or more jets and (b) 5 or more jets. The right ($t\bar{t}_R$) and wrong ($t\bar{t}_W$) combinations of $t\bar{t}$ events are shown separately, whereas all combinations are summed for $\bar{t}b$ and the backgrounds. The CC background curves in (a) are for electron and positron scattering using W^2 and Q^2 as parton cascade scale, whereas in (b) only the case of e^- with the W^2 scale is shown. The top quark mass is 60 GeV and events satisfy the requirements: eq. (12), no isolated lepton, $\sum E_\perp > 80$ GeV, circularity $C > 0.25$.

Figure 21 Twice differential distribution, $d^2\sigma/dm(j_1j_2j_3)dm(j_4j_5j_6)$, in the invariant masses of all possible combinations of two 3-jet systems from the 6-jet final state (obtained by forced reconstruction in events with at least 4 original jets). (a) NC+CC backgrounds, (b) $\bar{t}b$ events, (c) wrong and (d) right jet combinations in $t\bar{t}$ events. Conditions and notations as in Fig. 20.

Figure 22 As Fig. 20, but after taking only those groupings of 6-jet non-leptonic events where both 3-jet masses fall in the 'window' m(3-jet) $\in [57, 63]$ GeV. Otherwise conditions and notations as in Fig. 20.

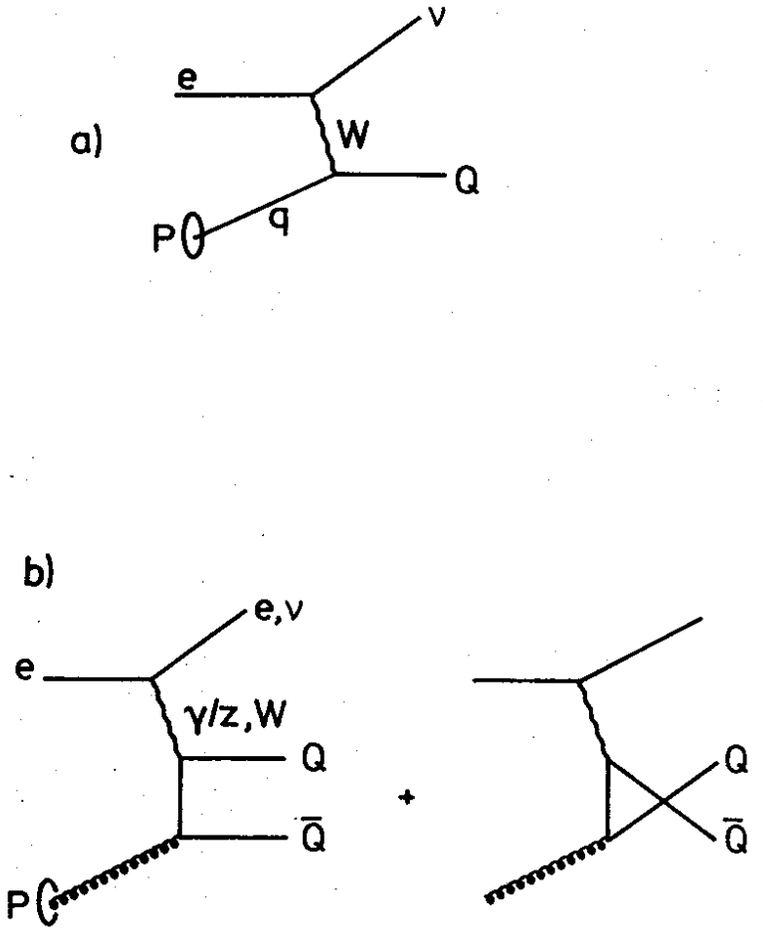
a)
e
ν
W
Q
P
q
b)
e
e,ν
γ/z,W
Q
Q̄
P
+
Q
Q̄

Fig.1

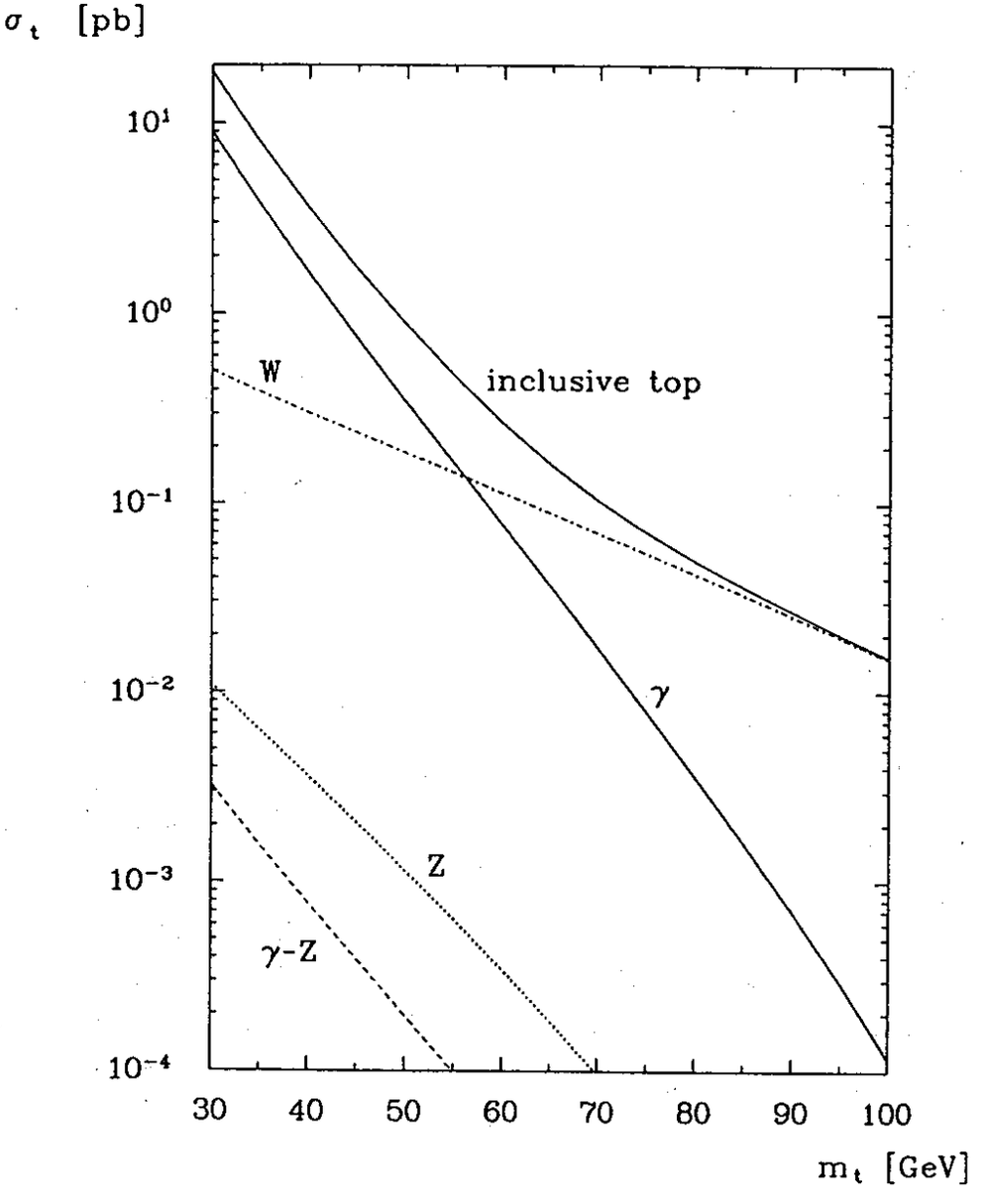
σ_t [pb]
10¹
10⁰
10⁻¹
10⁻²
10⁻³
10⁻⁴
W
inclusive top
γ
Z
γ-Z
30
40
50
60
70
80
90
100
m_t [GeV]

Fig. 2

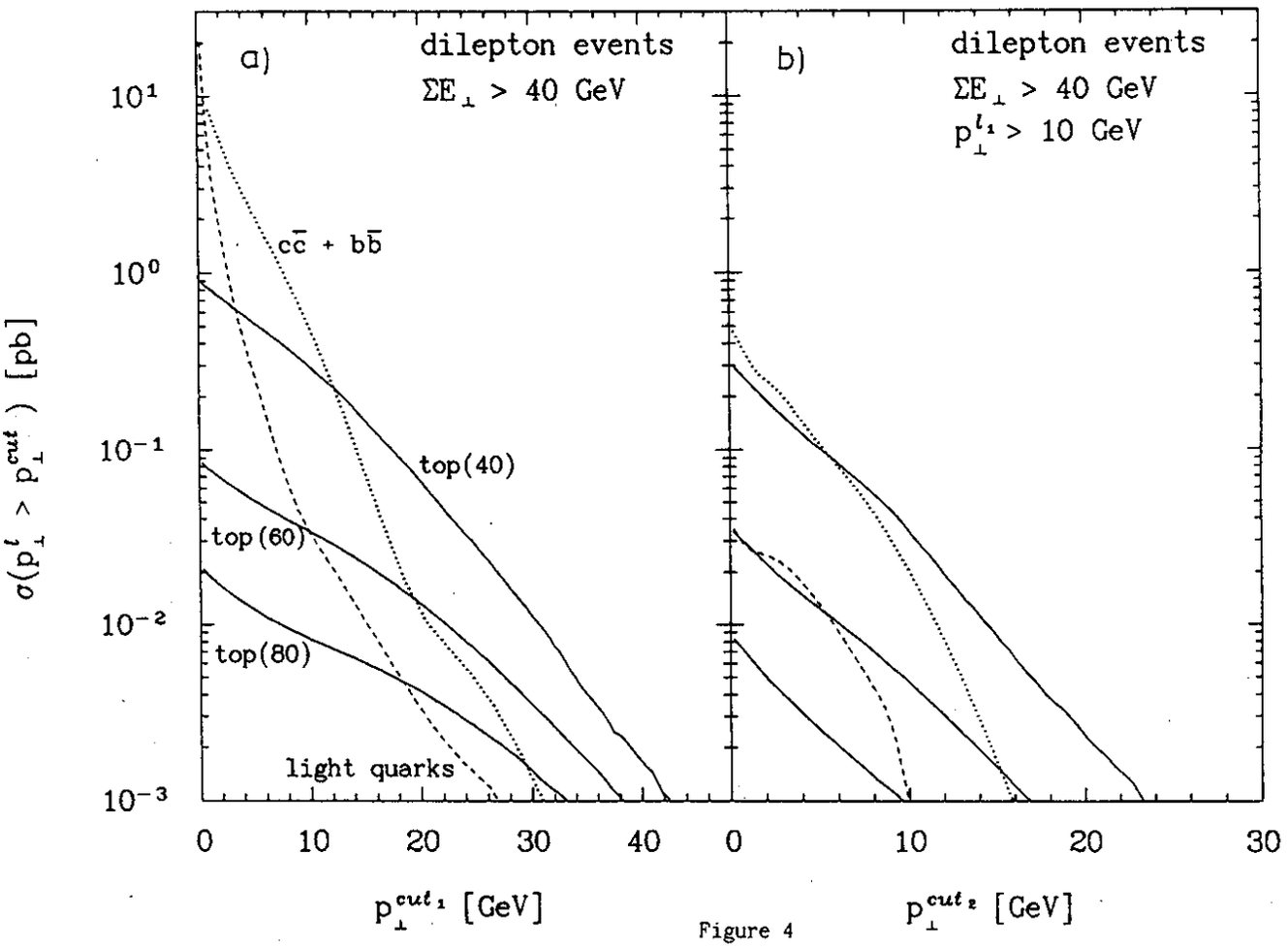

Figure 4

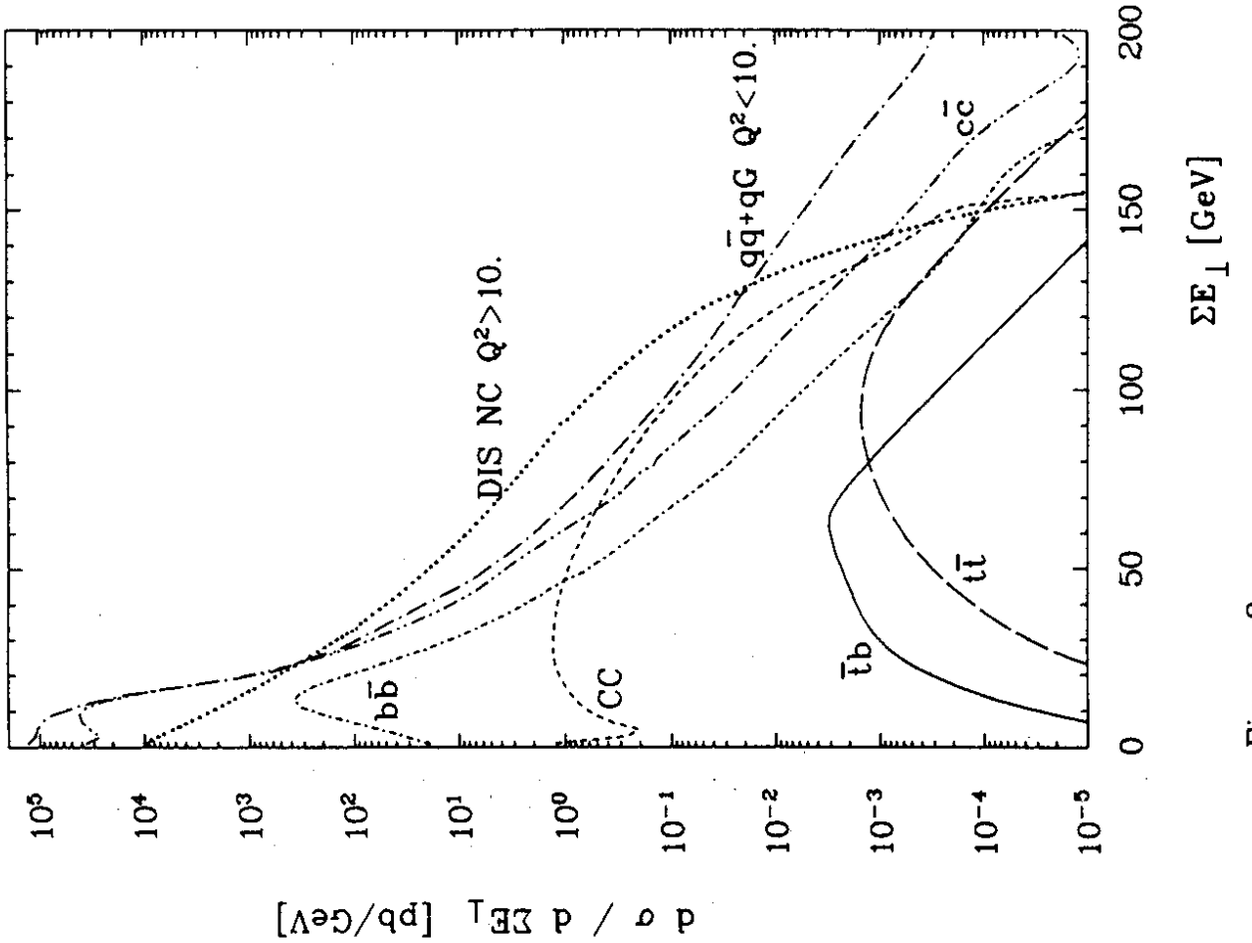

Figure 3

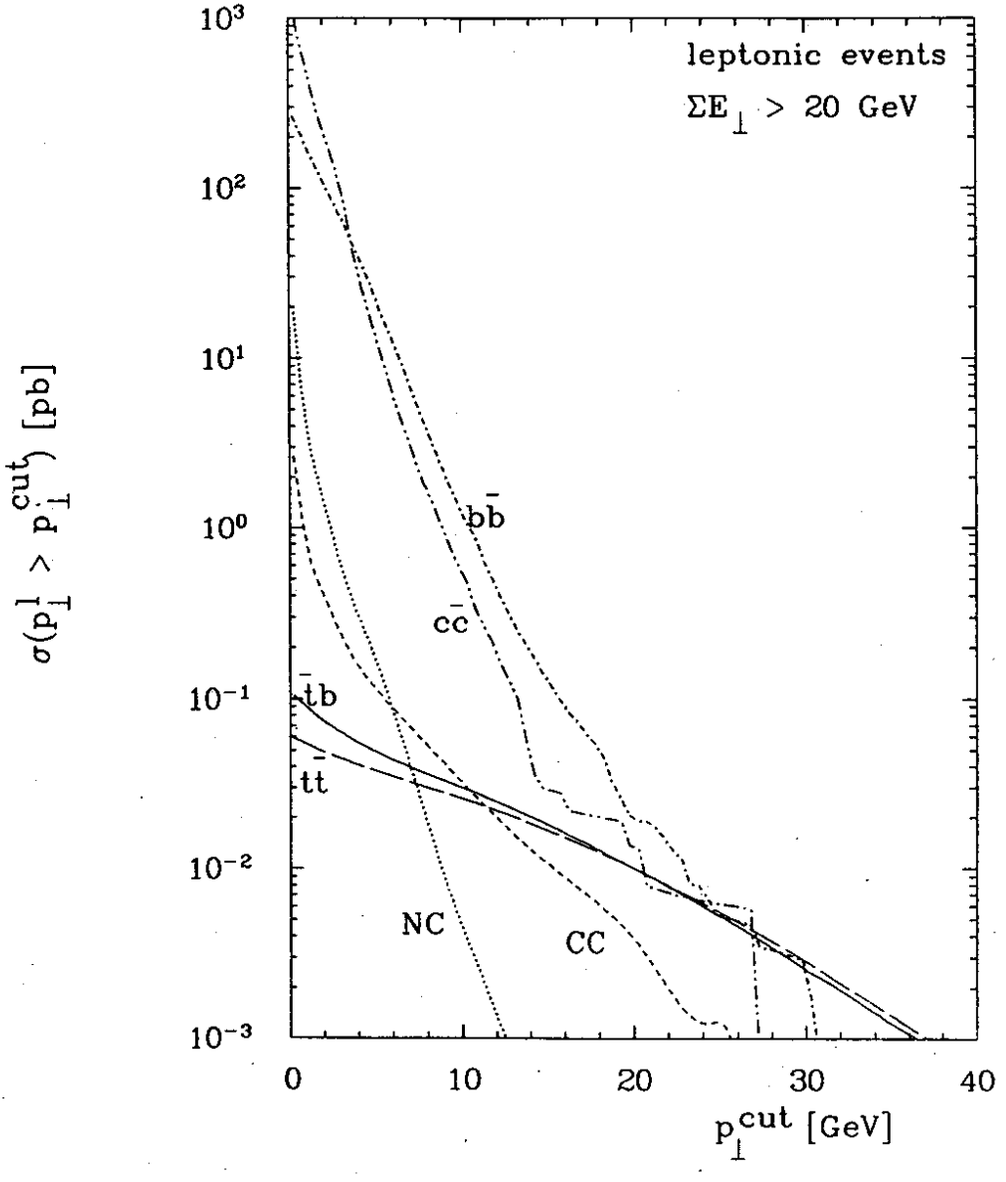

Figure 5

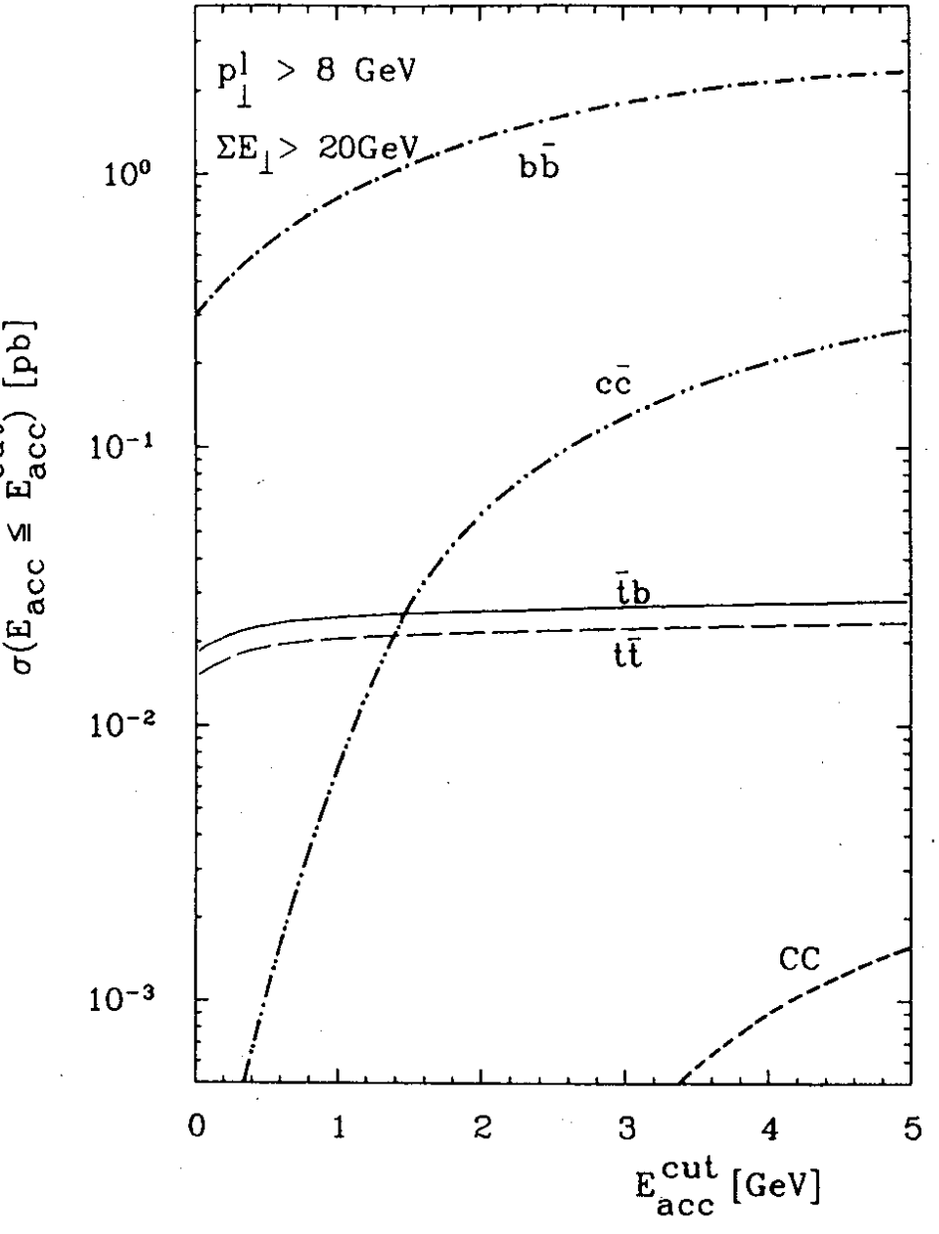

Figure 6

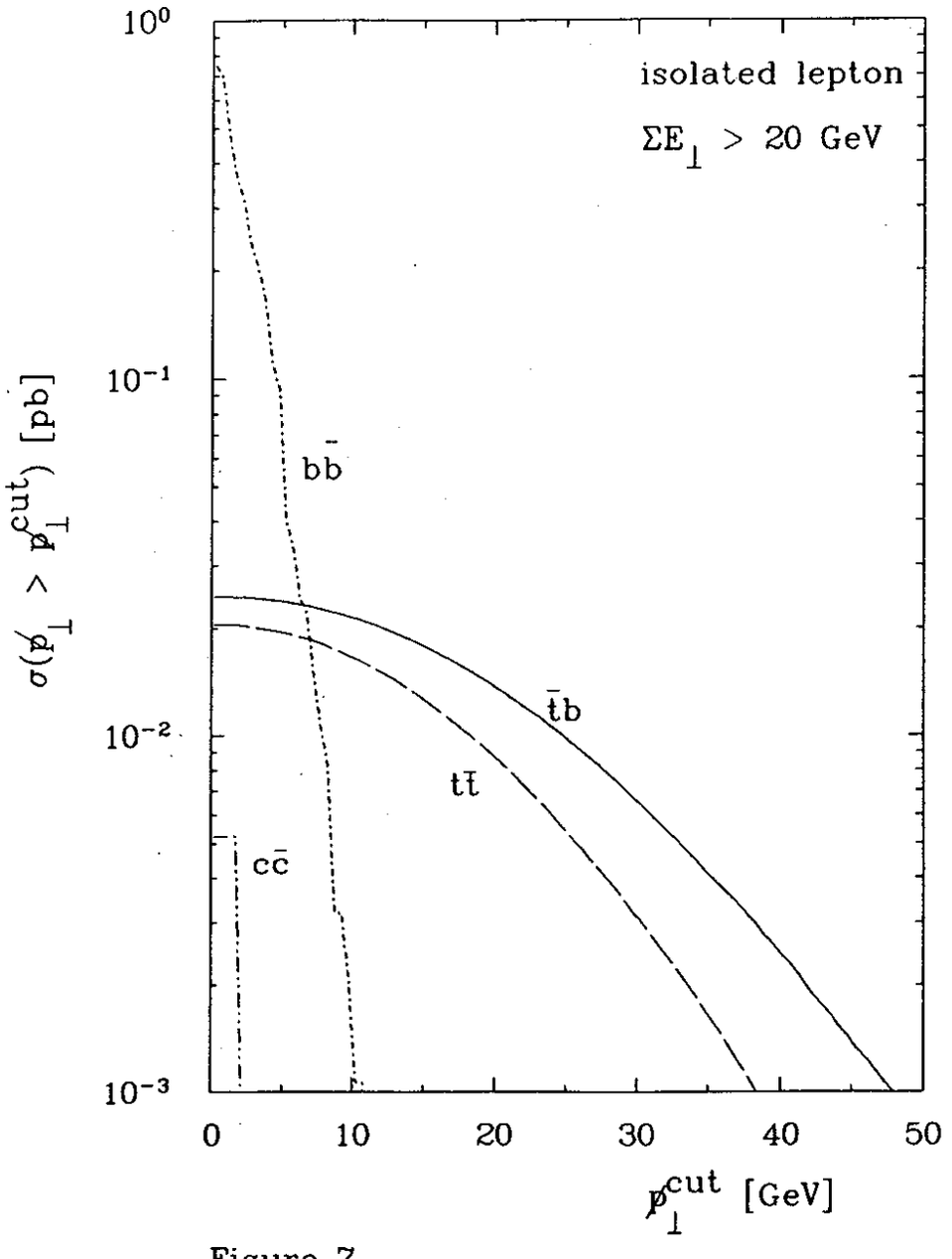

Figure 7

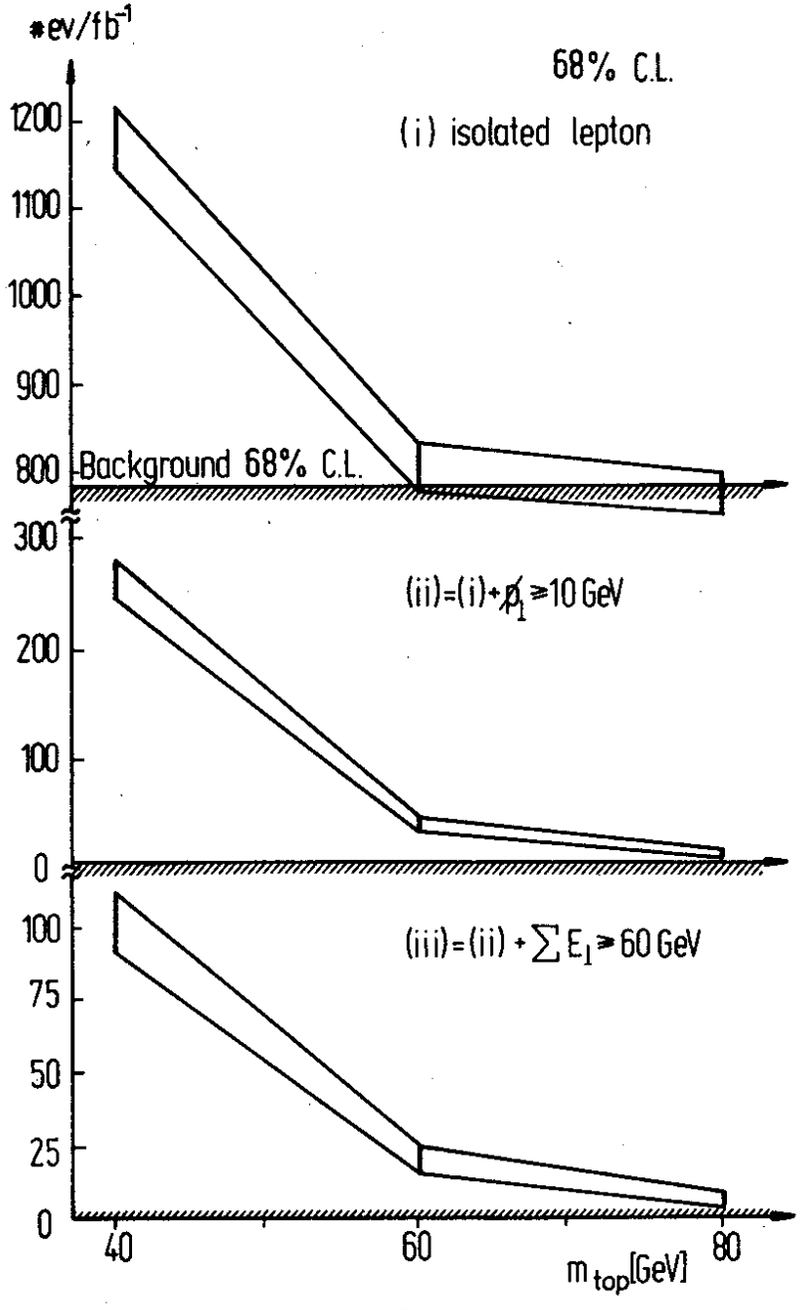

Fig.8

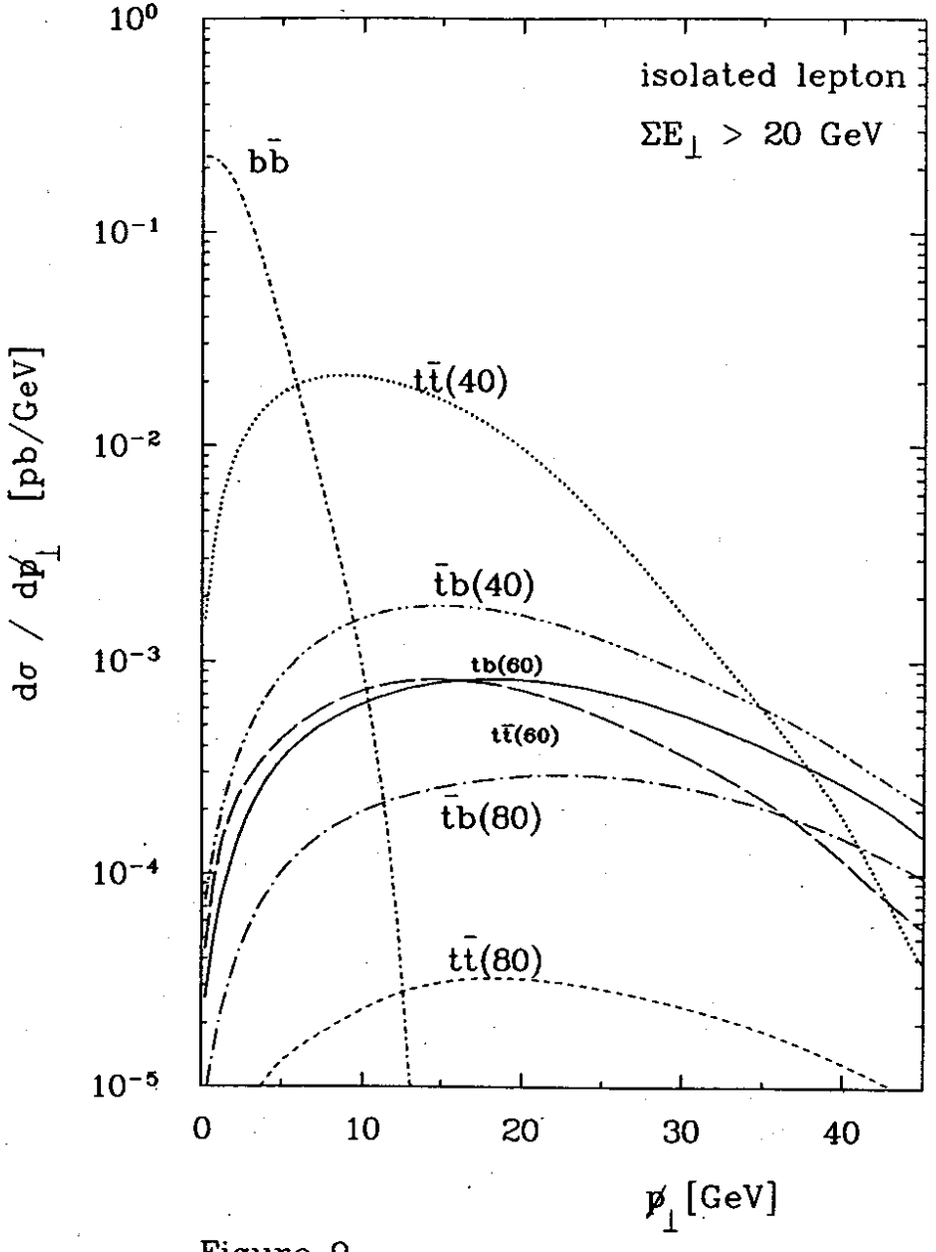

Figure 9

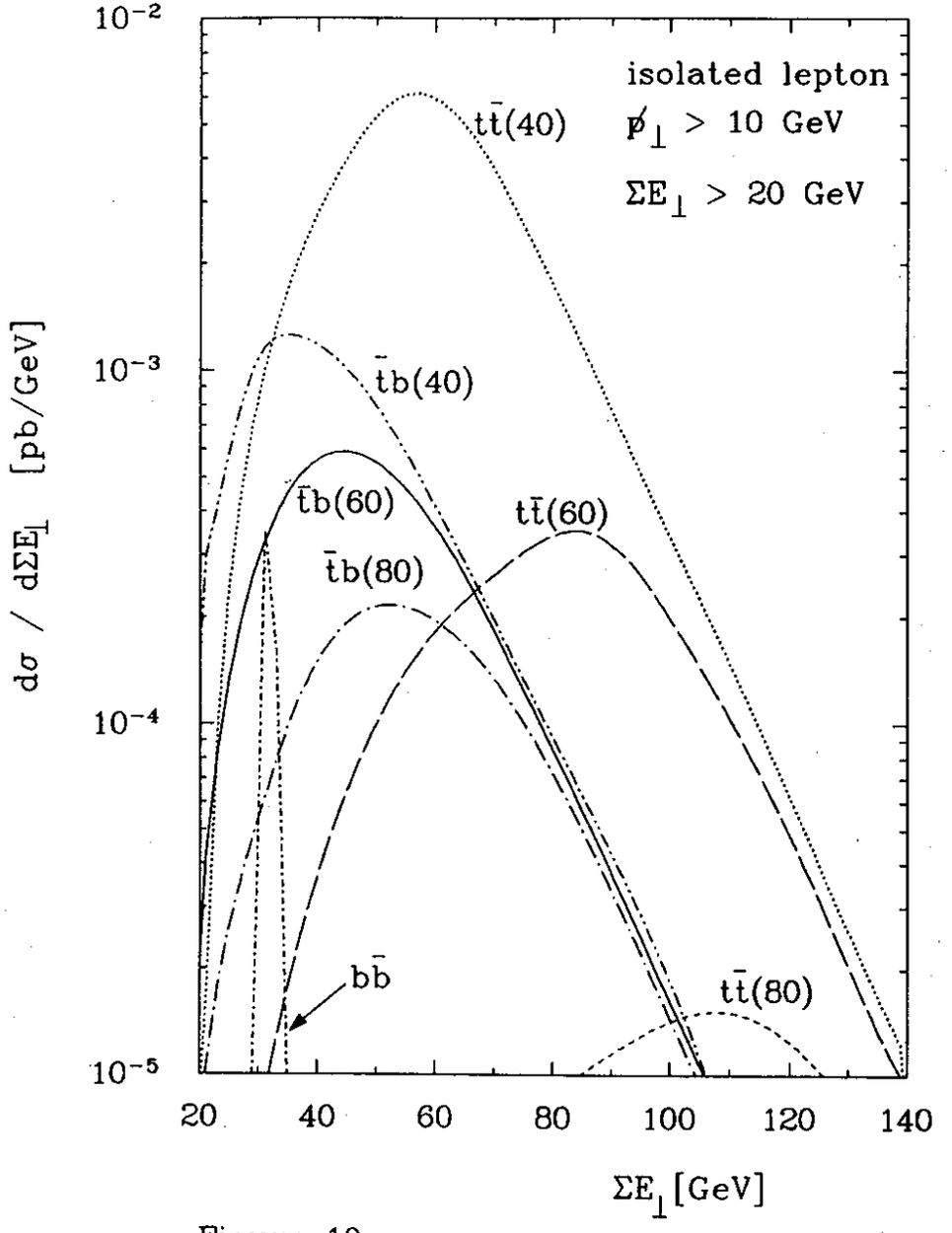

Figure 10

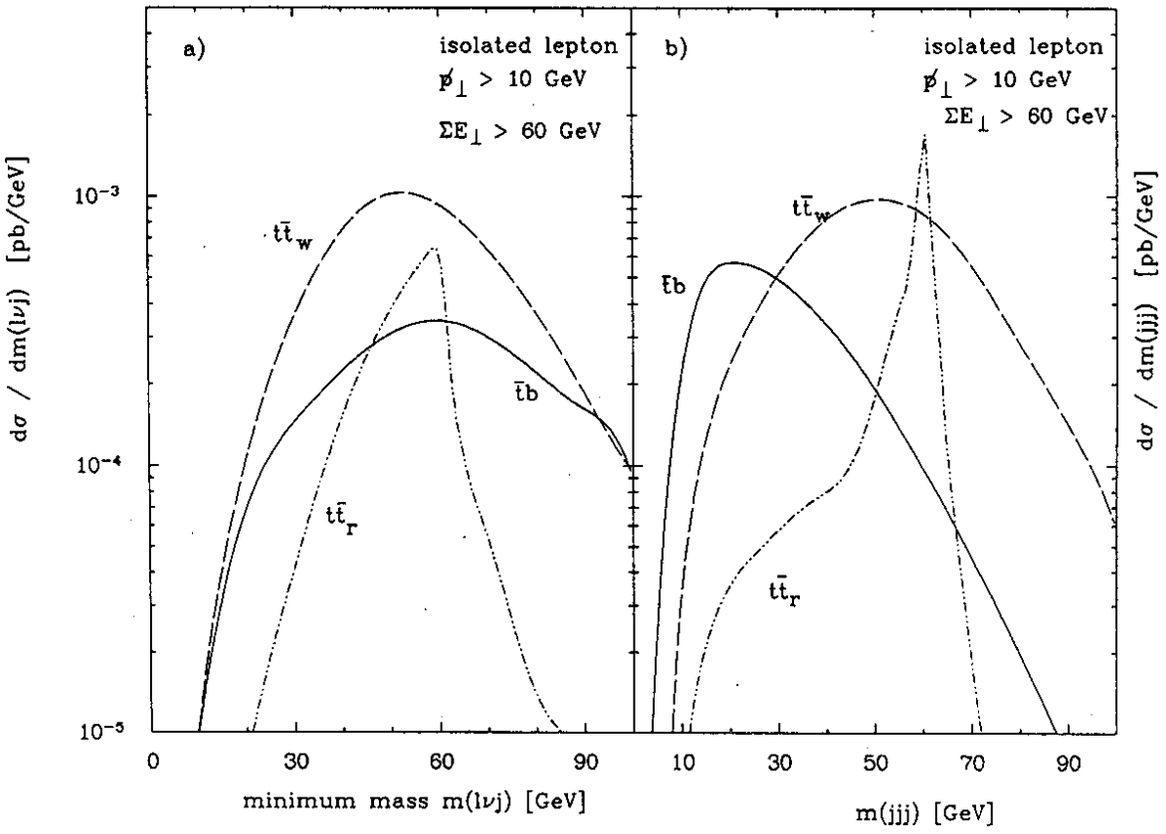

Figure 12

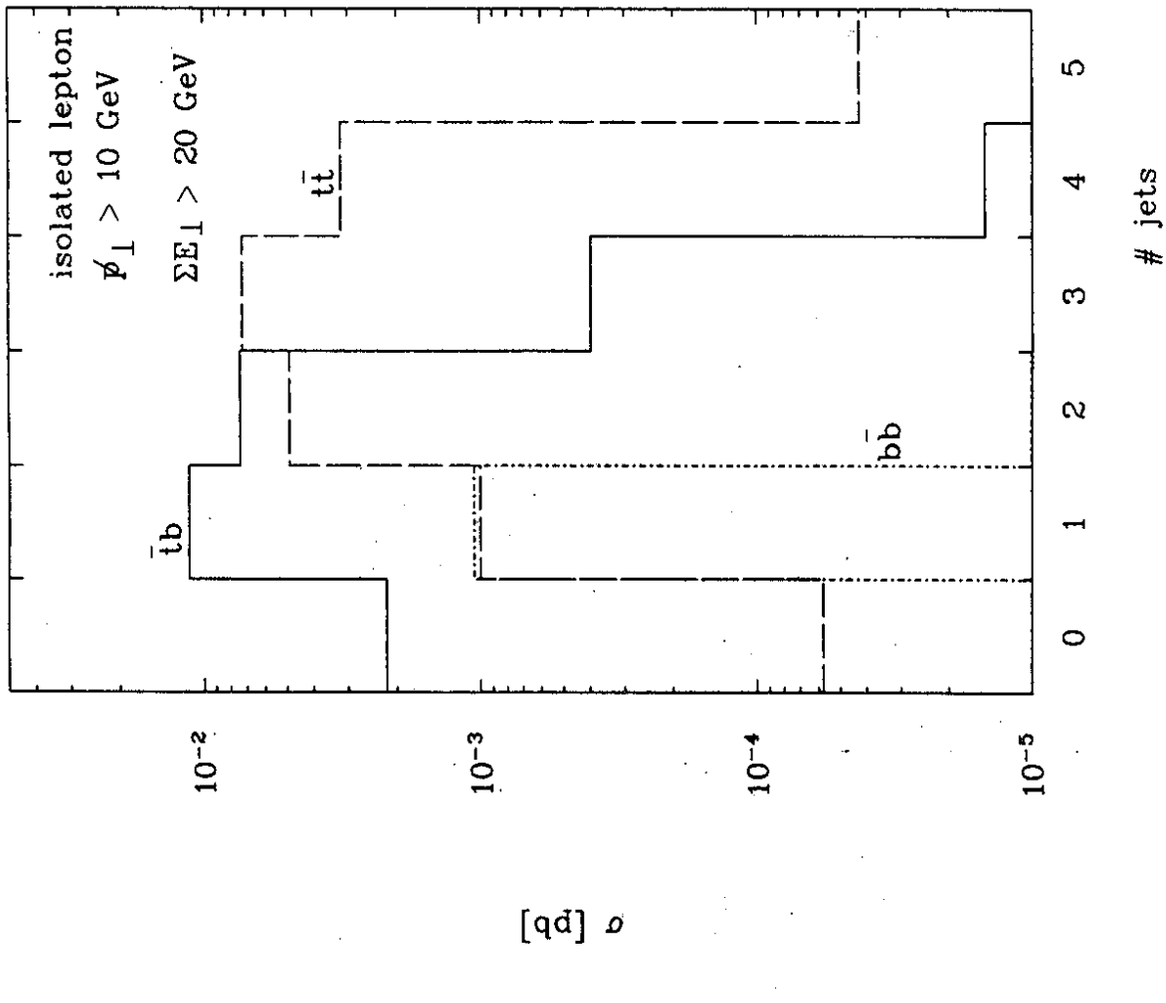

Figure 11

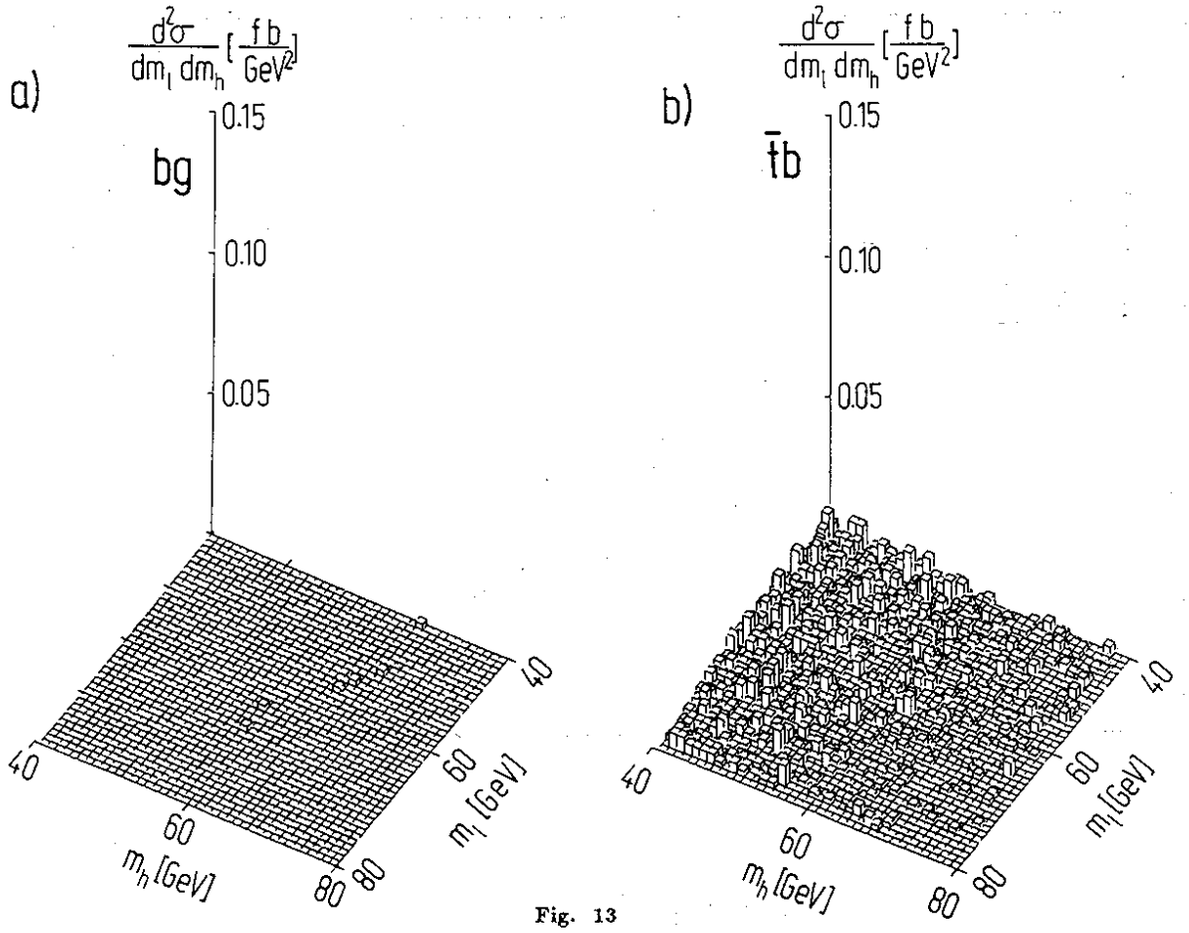
a)
$\frac{d^2\sigma}{dm_t\,dm_h}\,[\frac{fb}{GeV^2}]$
bg
0.15
0.10
0.05
40
60
80
m_h [GeV]
m_t [GeV]
b)
$\bar{t}b$

Fig. 13

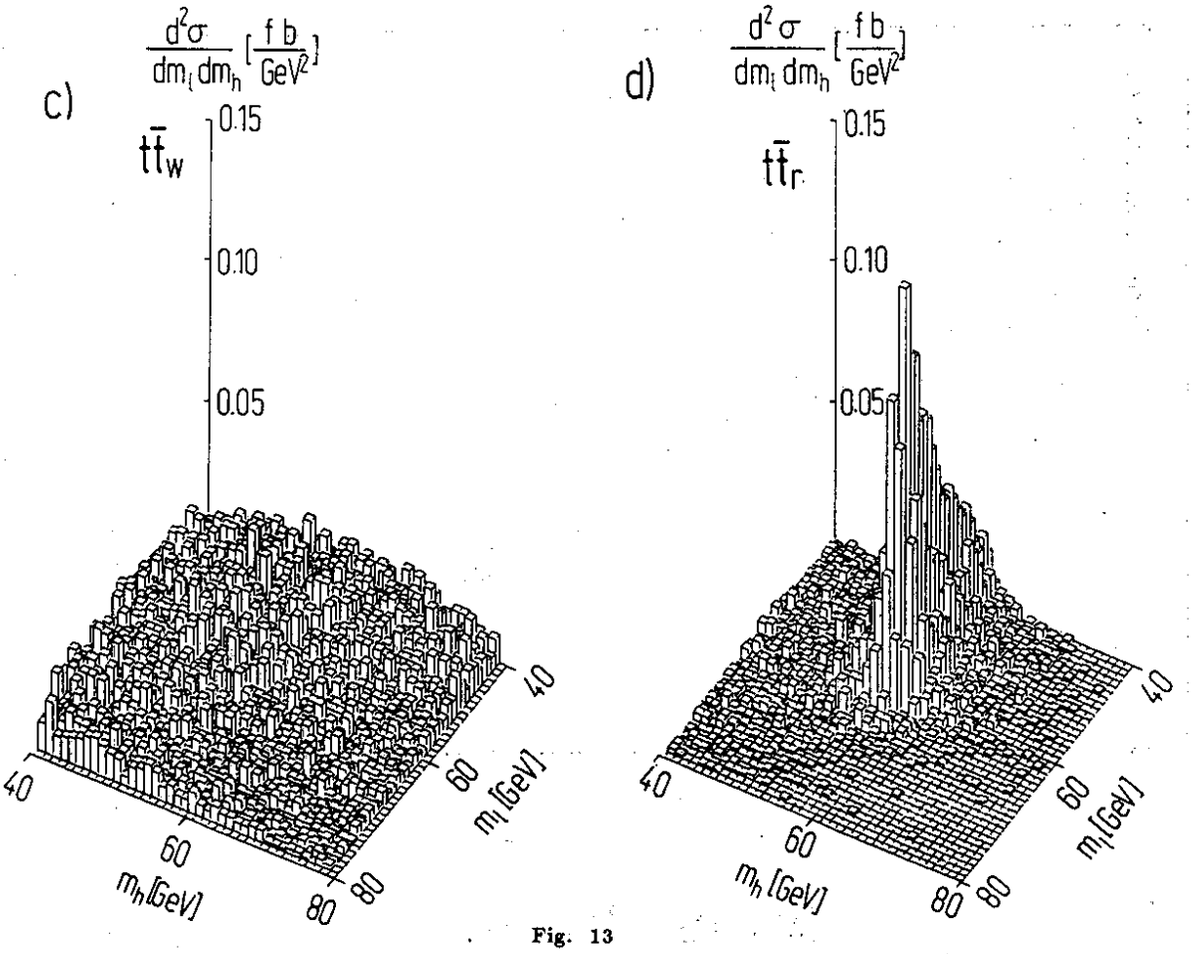
c)
$\frac{d^2\sigma}{dm_t\,dm_h}\,[\frac{fb}{GeV^2}]$
$t\bar{t}_W$
0.15
0.10
0.05
40
60
80
m_h [GeV]
m_t [GeV]
d)
$t\bar{t}_\Gamma$

Fig. 13

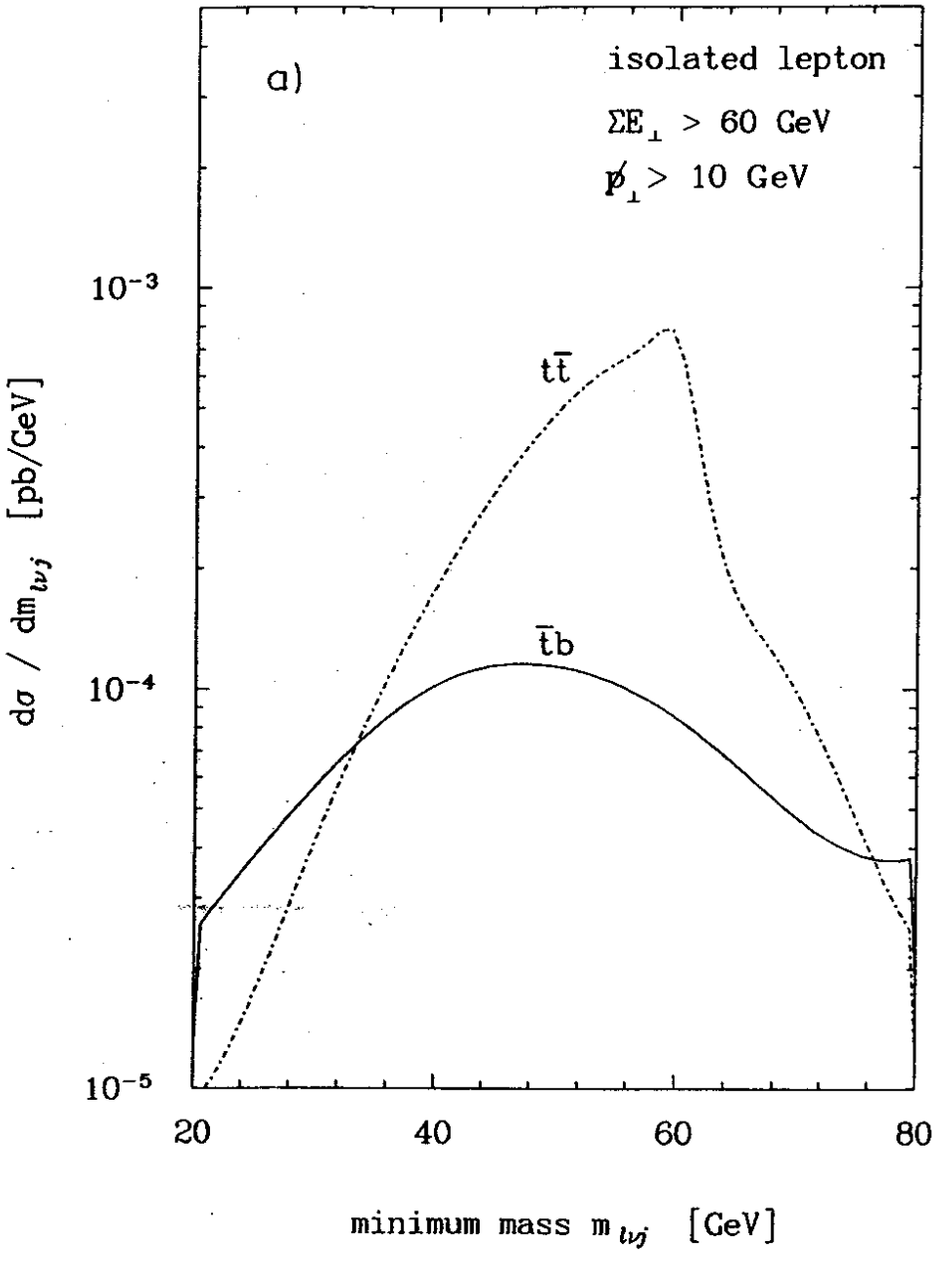

Figure 14 (a)

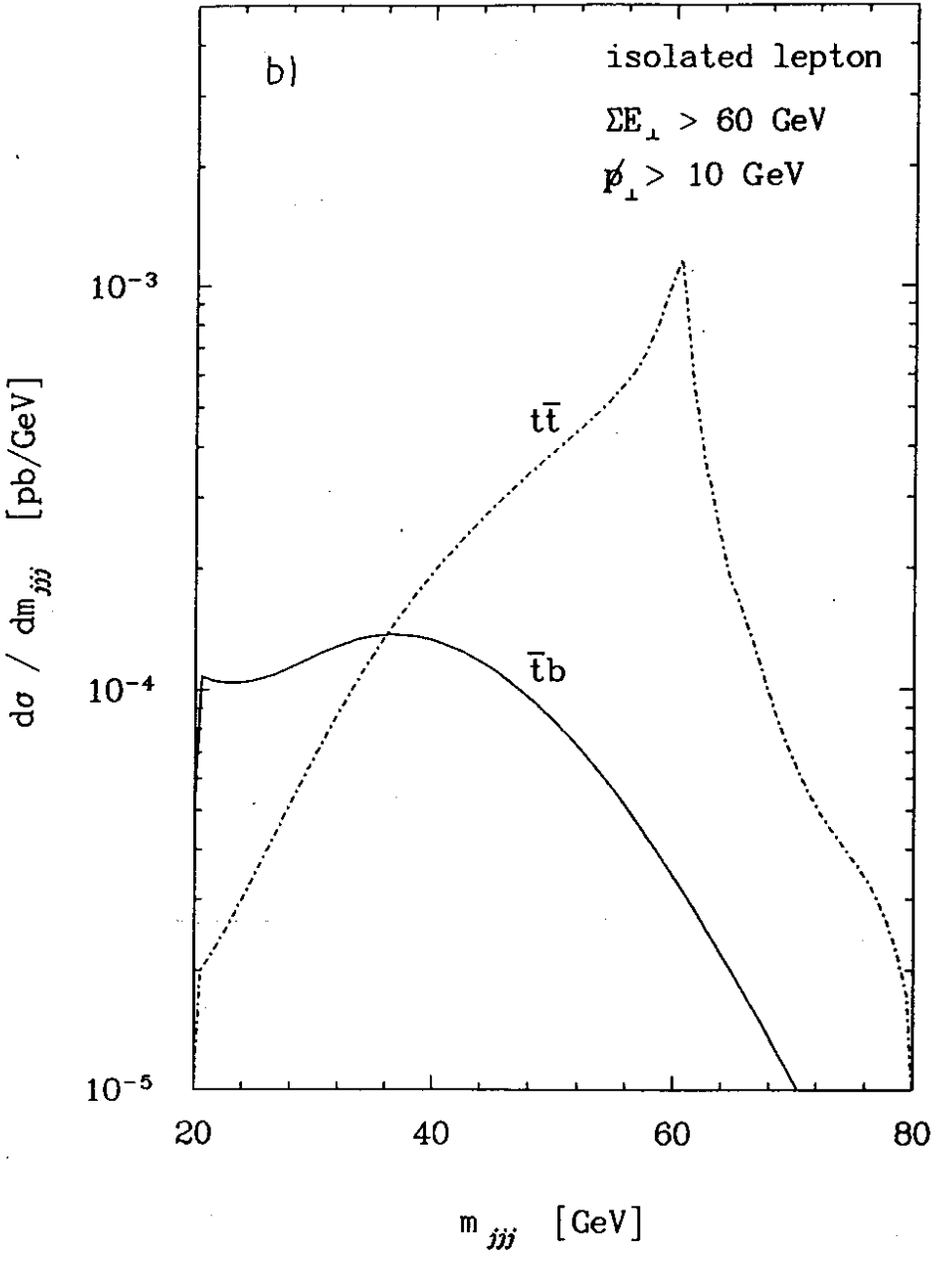

Figure 14 (b)

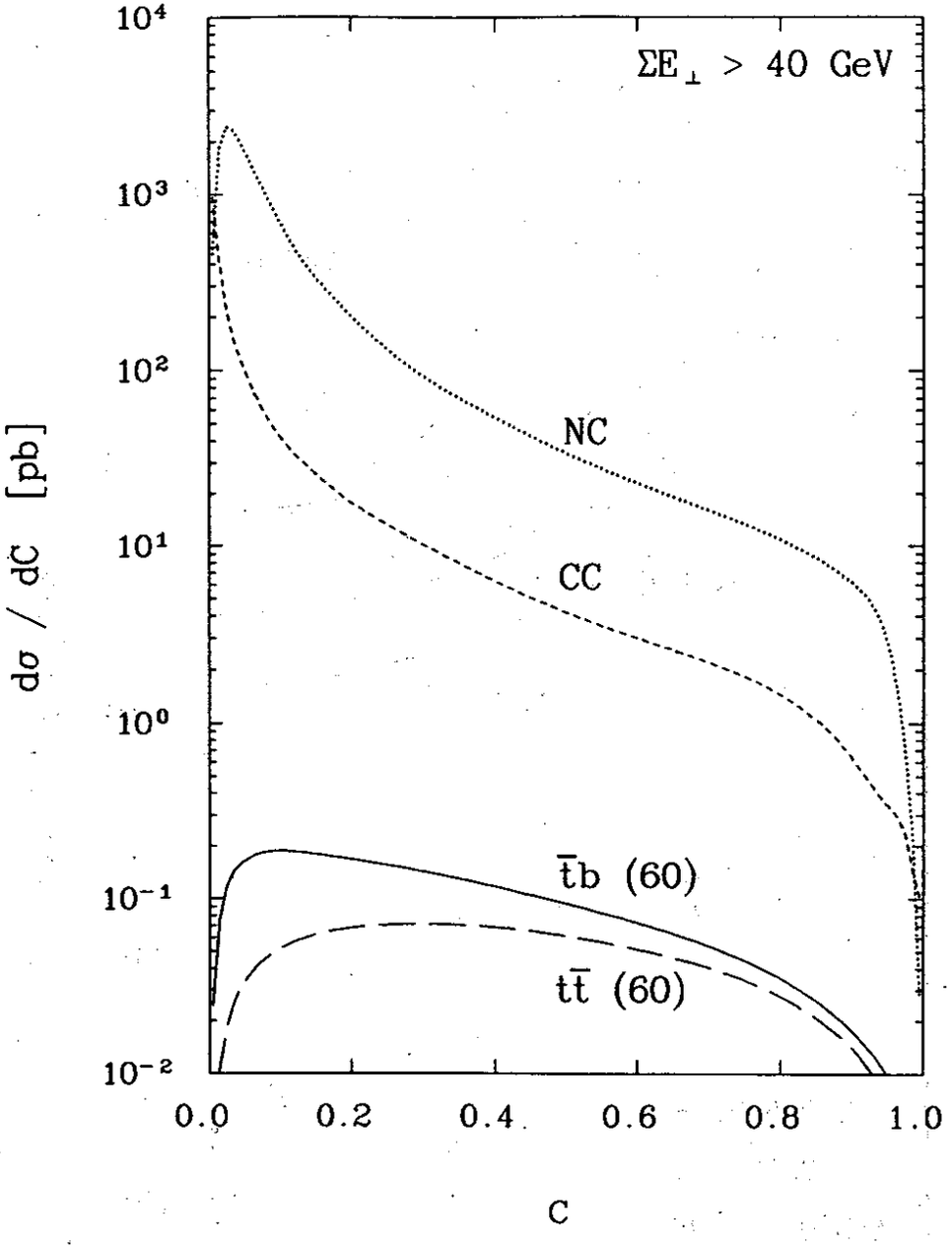

Figure 15

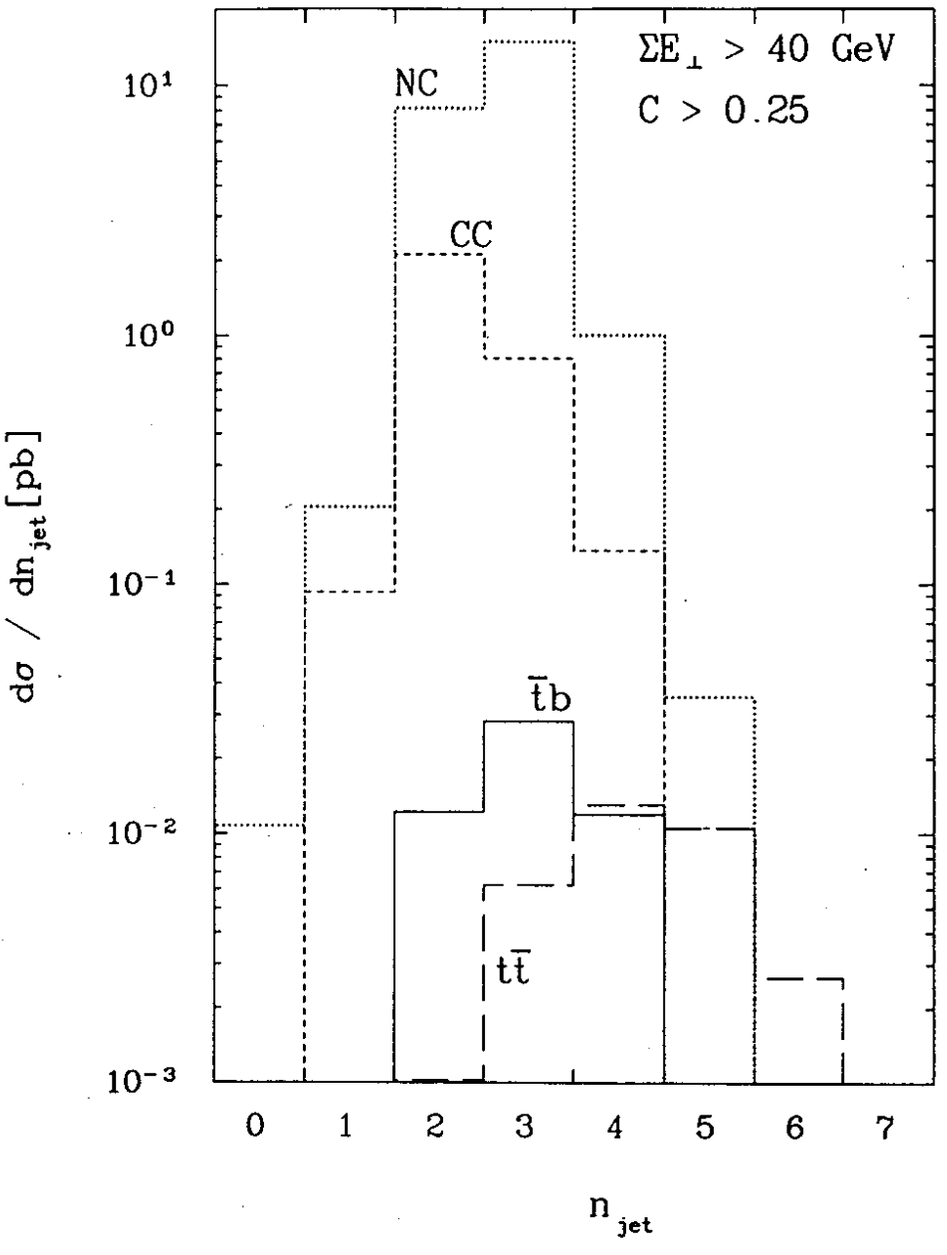

Figure 16

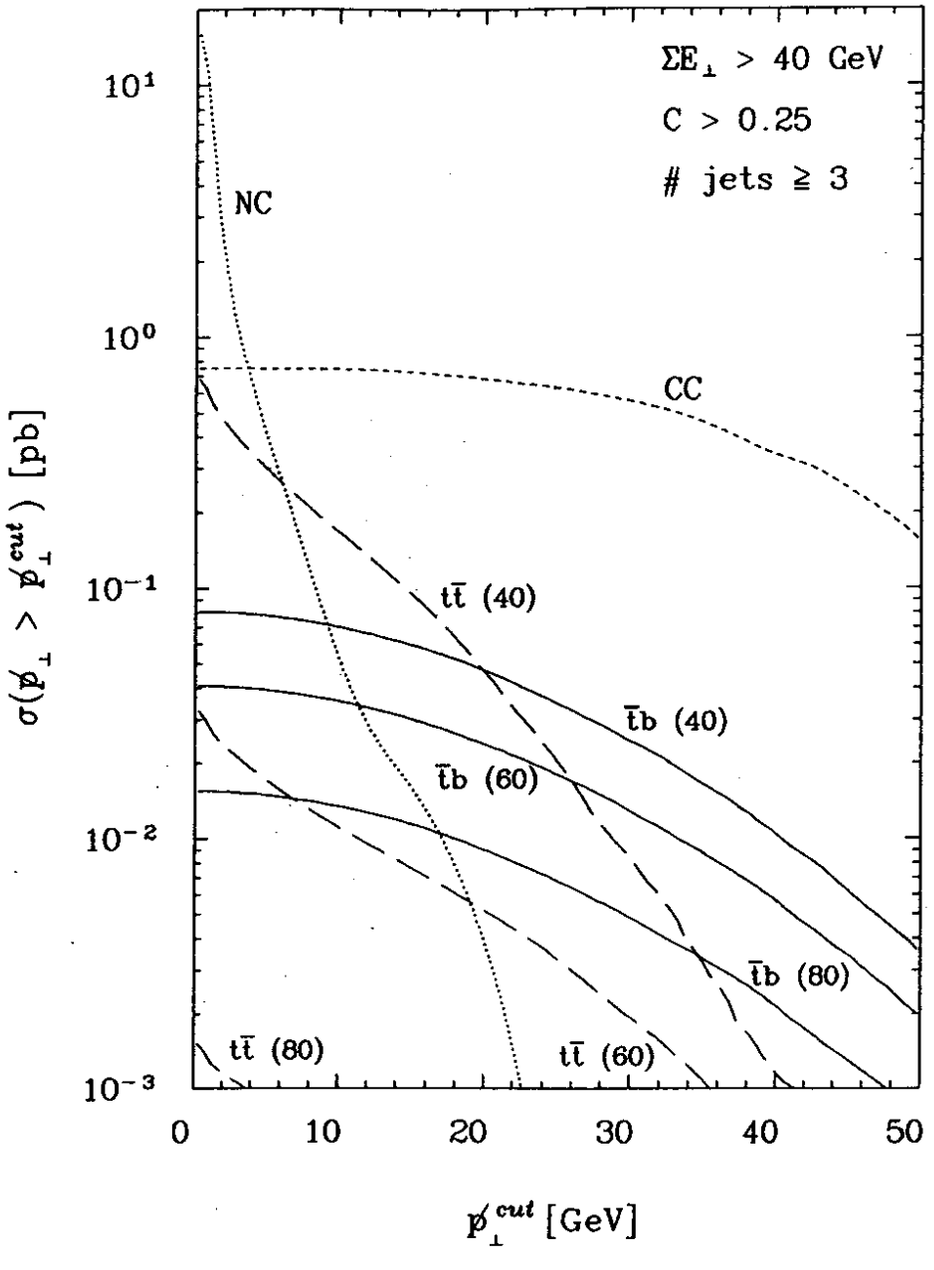
ΣE⊥ > 40 GeV
C > 0.25
jets ≧ 3
NC
CC
tt̄ (40)
b̄b (40)
b̄b (60)
b̄b (80)
tt̄ (80)
tt̄ (60)
10¹
10⁰
10⁻¹
10⁻²
10⁻³
0
10
20
30
40
50
σ(p⊥ > p⊥cut) [pb]
p⊥cut [GeV]

Figure 17

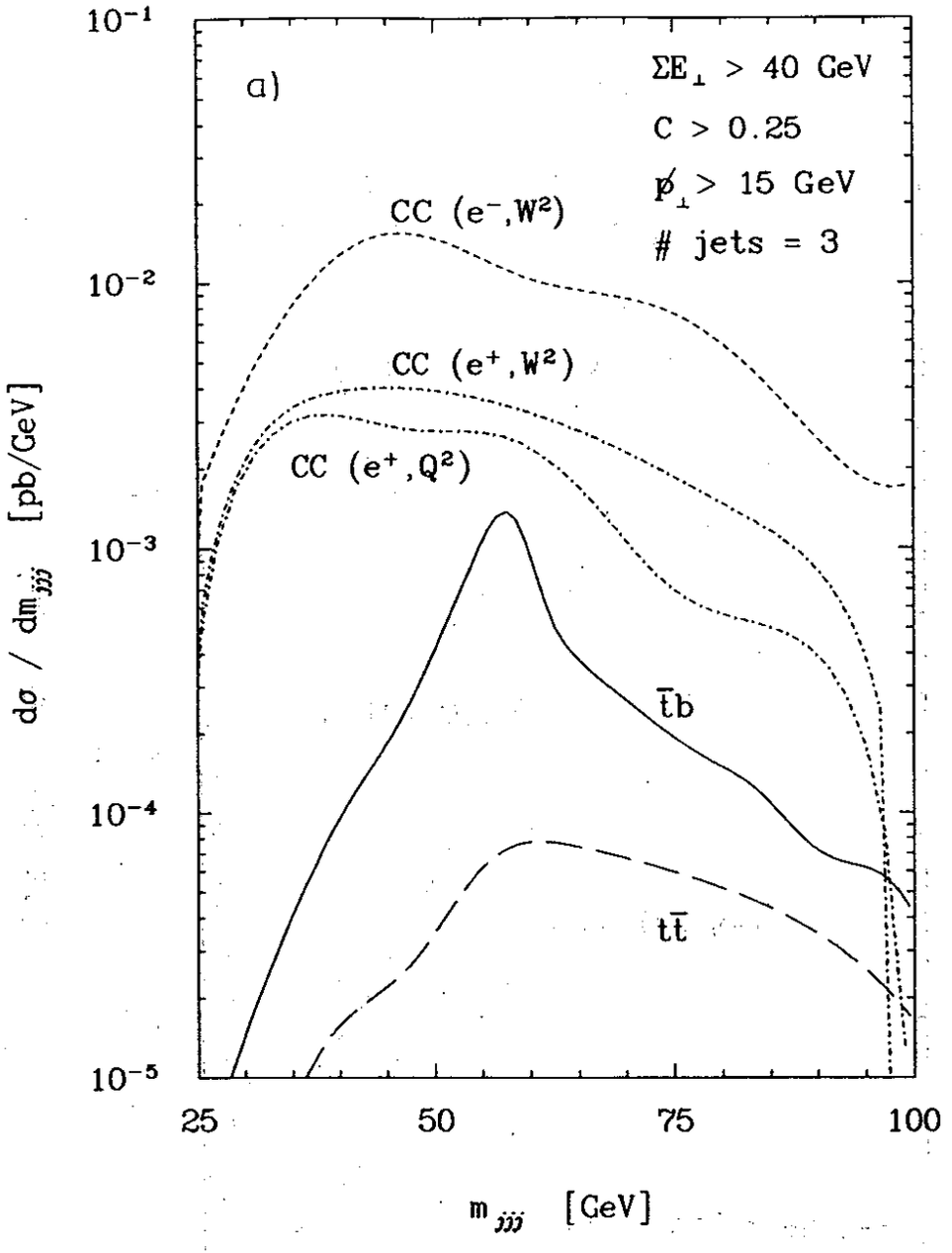

Figure 18 (a)

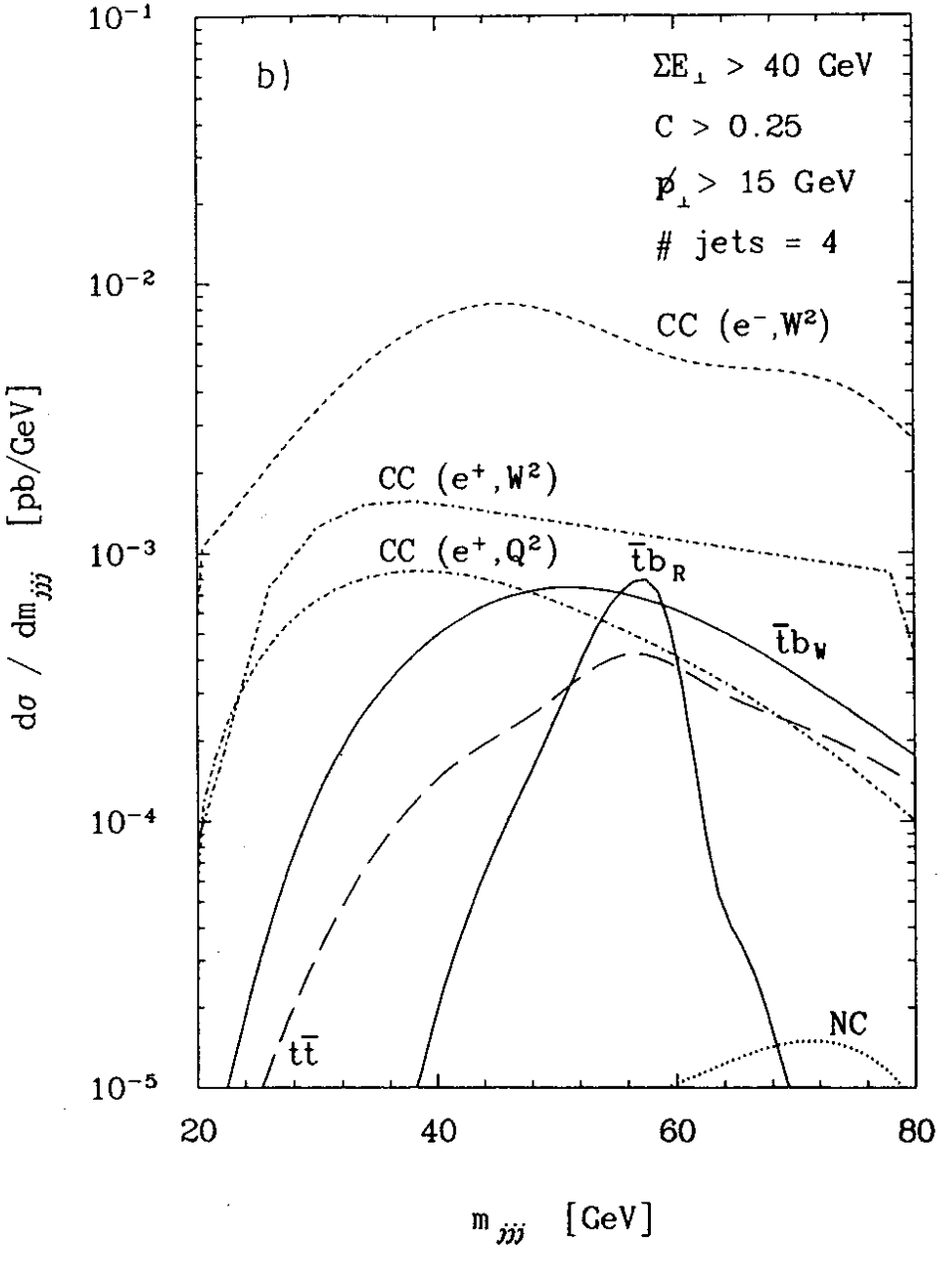

Figure 18 (b)

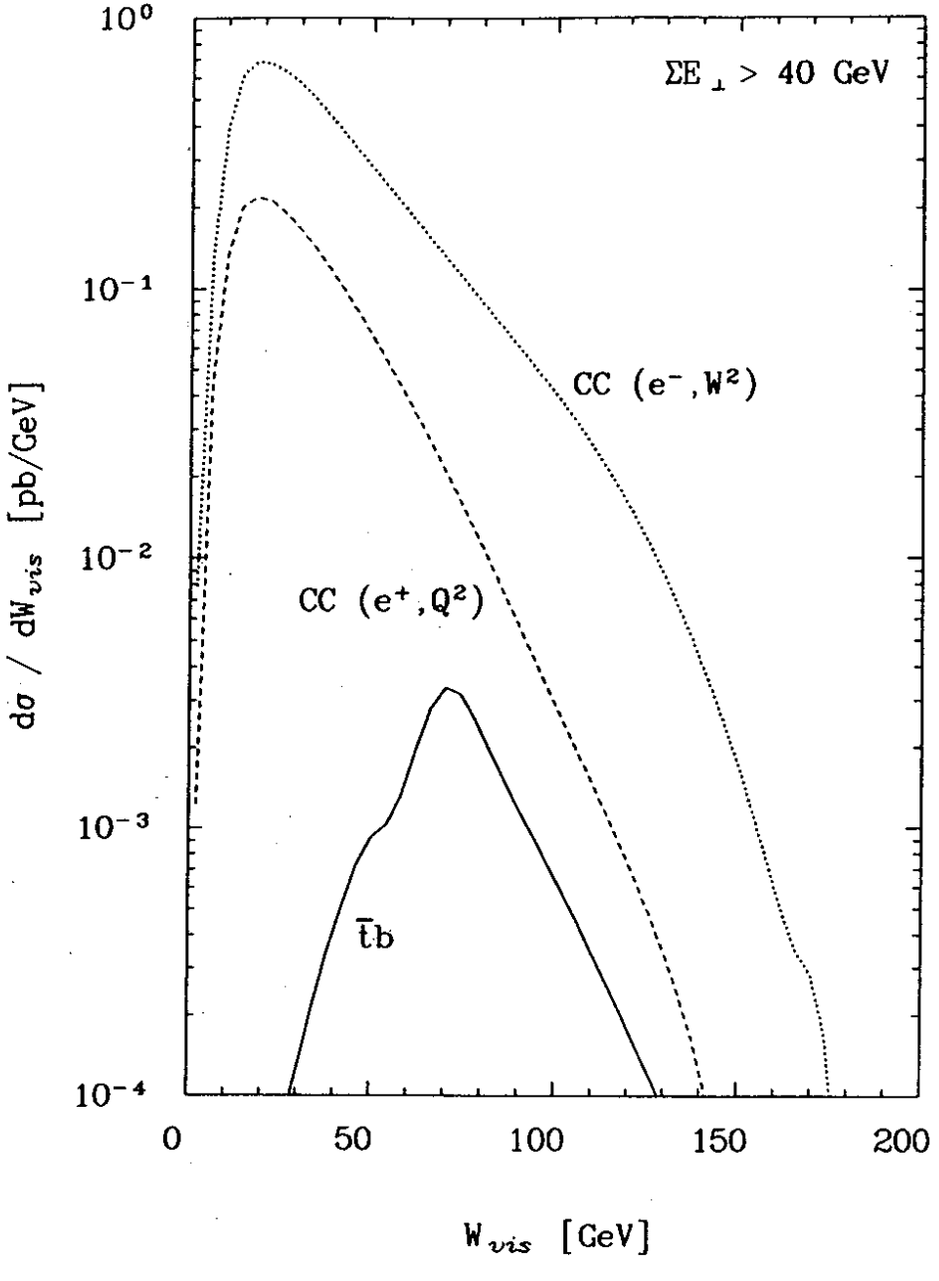
10^0
10^{-1}
10^{-2}
10^{-3}
10^{-4}
$\Sigma E_\perp > 40$ GeV
CC (e^-, W^2)
CC (e^+, Q^2)
$\bar{t}b$
0
50
100
150
200
$d\sigma / dW_{vis}$ [pb/GeV]
W_{vis} [GeV]

Figure 19

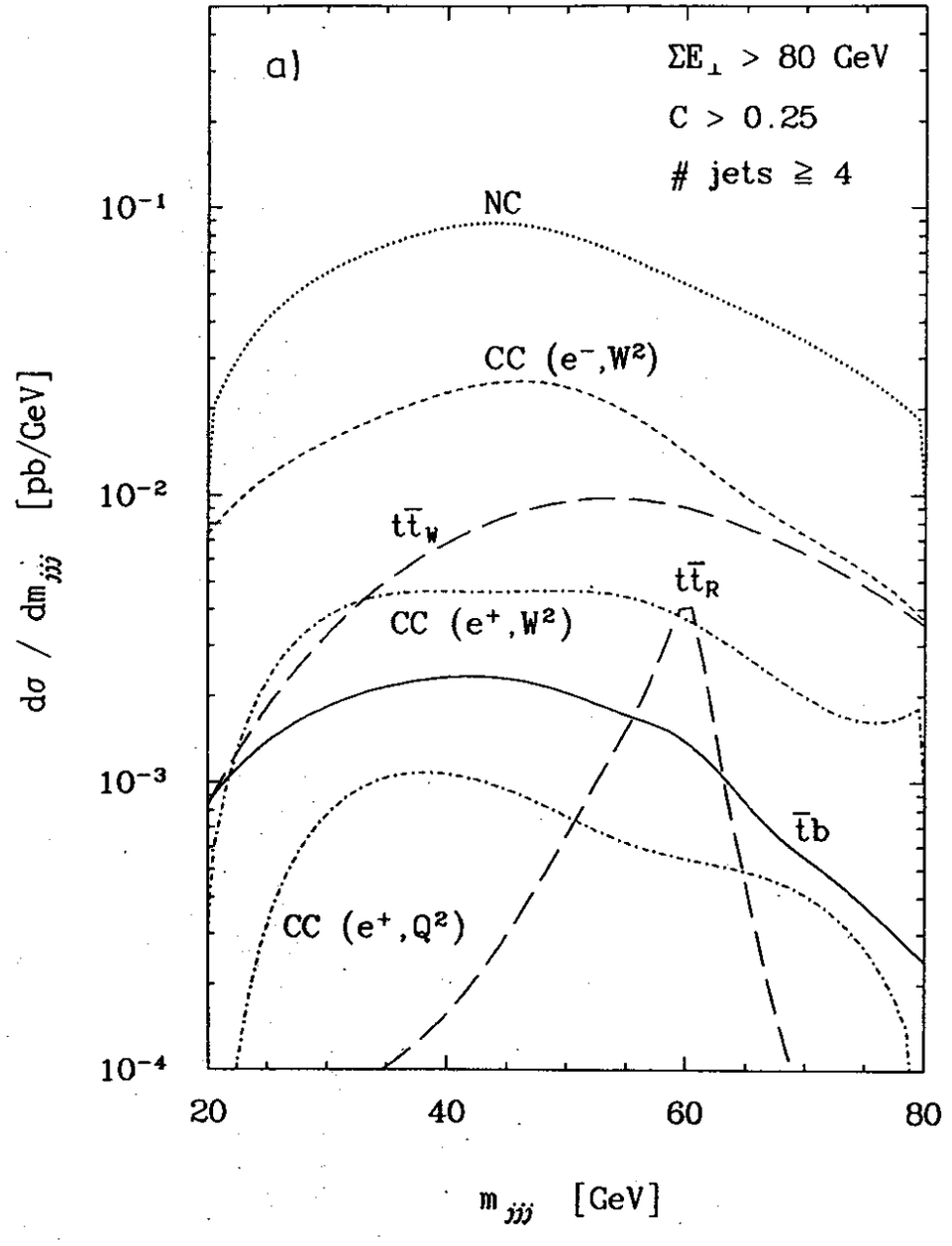

Figure 20 (a)

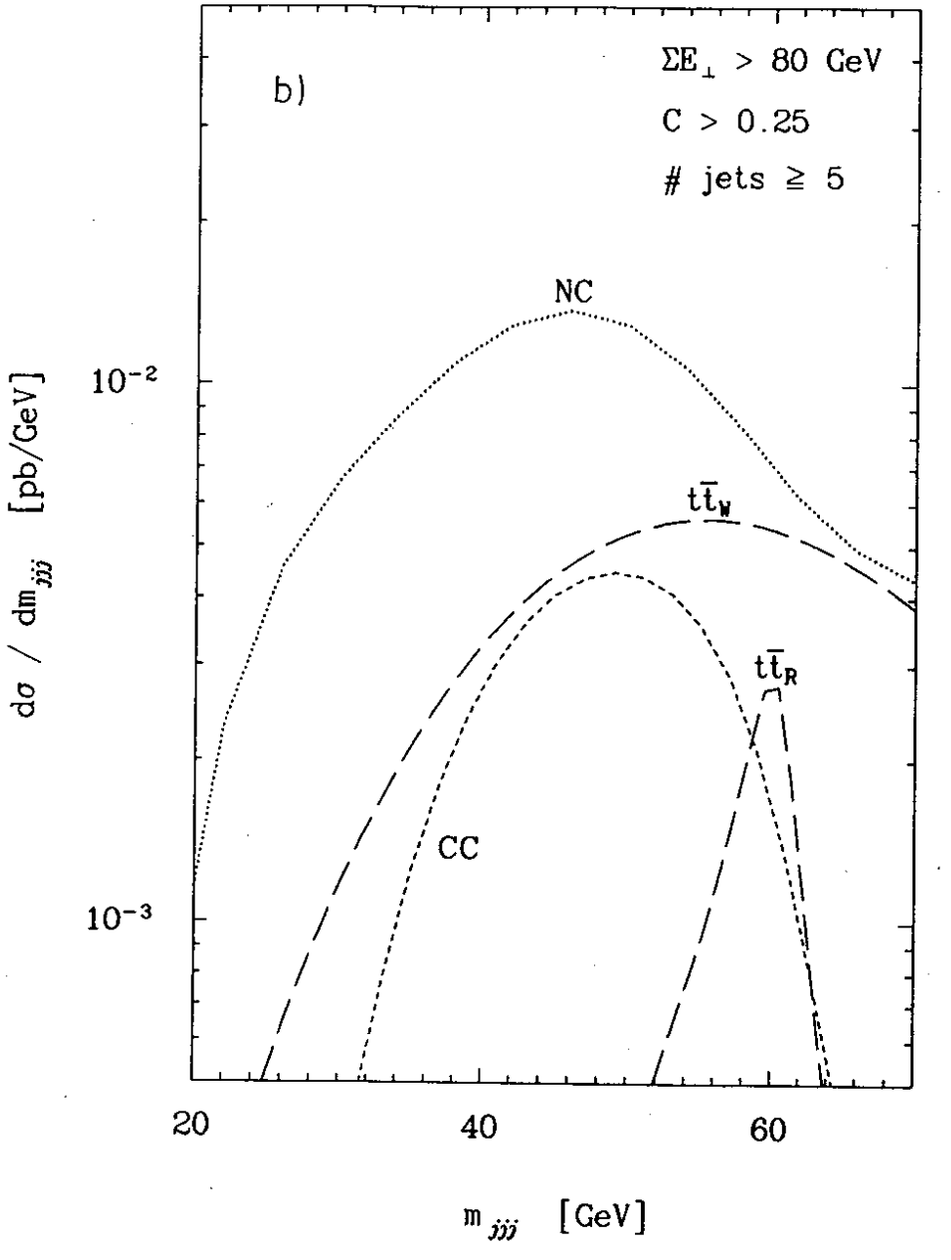

Figure 20 (b)

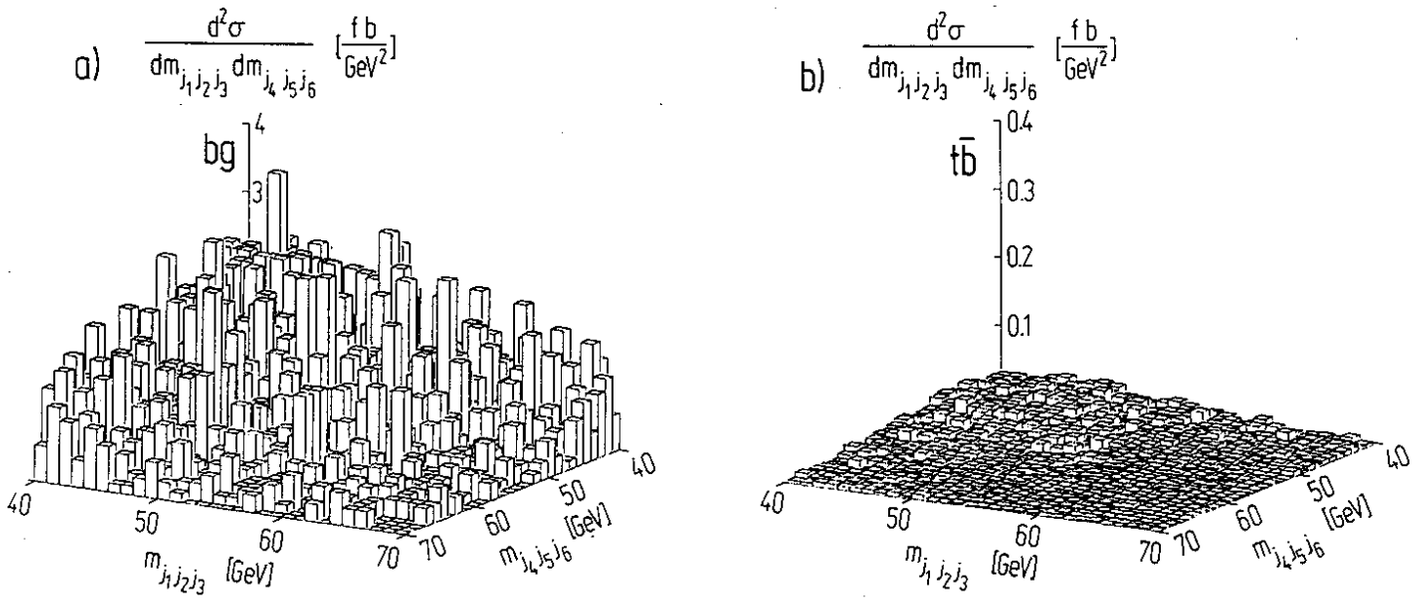
a)
$\frac{d^2\sigma}{dm_{j_1 j_2 j_3}\, dm_{j_4 j_5 j_6}}$ $[\frac{fb}{GeV^2}]$
bg
4
3
40
50
60
70
$m_{j_1 j_2 j_3}$ [GeV]
$m_{j_4 j_5 j_6}$ [GeV]
b)
$\frac{d^2\sigma}{dm_{j_1 j_2 j_3}\, dm_{j_4 j_5 j_6}}$ $[\frac{fb}{GeV^2}]$
$t\bar{b}$
0.4
0.3
0.2
0.1
40
50
60
70
$m_{j_1 j_2 j_3}$ [GeV]
$m_{j_4 j_5 j_6}$ [GeV]

Fig. 21

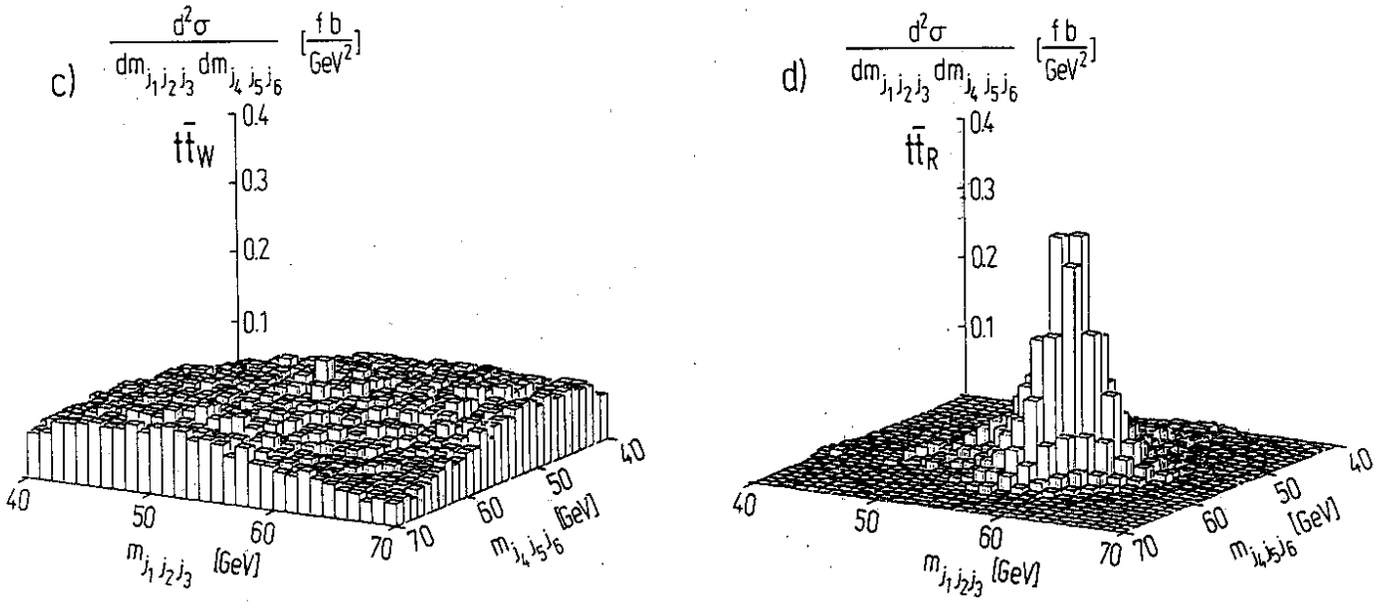
c)
$\frac{d^2\sigma}{dm_{j_1 j_2 j_3}\, dm_{j_4 j_5 j_6}}$ $[\frac{fb}{GeV^2}]$
$t\bar{t}_W$
0.4
0.3
0.2
0.1
40
50
60
70
$m_{j_1 j_2 j_3}$ [GeV]
$m_{j_4 j_5 j_6}$ [GeV]
d)
$\frac{d^2\sigma}{dm_{j_1 j_2 j_3}\, dm_{j_4 j_5 j_6}}$ $[\frac{fb}{GeV^2}]$
$t\bar{t}_R$
0.4
0.3
0.2
0.1
40
50
60
70
$m_{j_1 j_2 j_3}$ [GeV]
$m_{j_4 j_5 j_6}$ [GeV]

Fig. 21

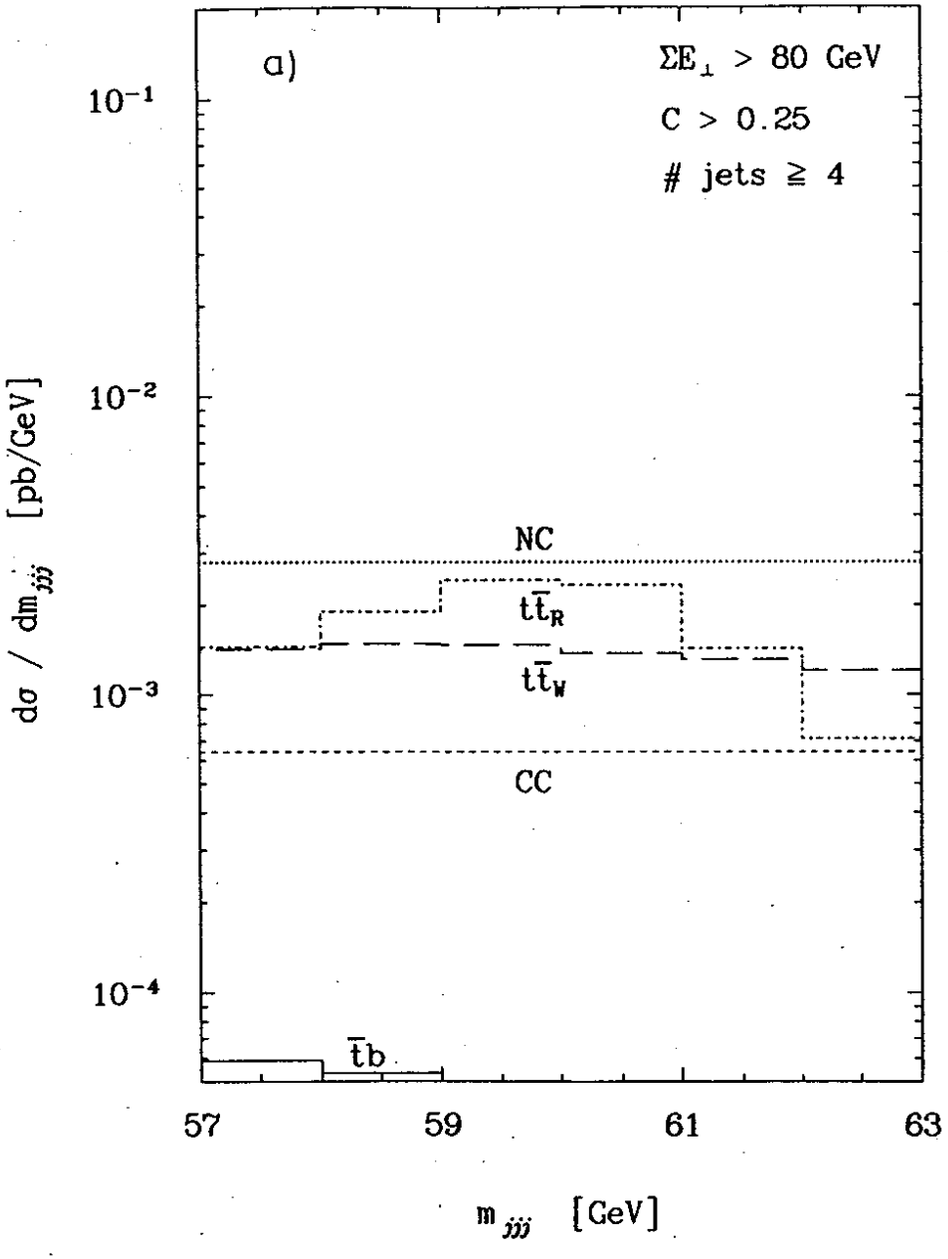

Figure 22 (a)

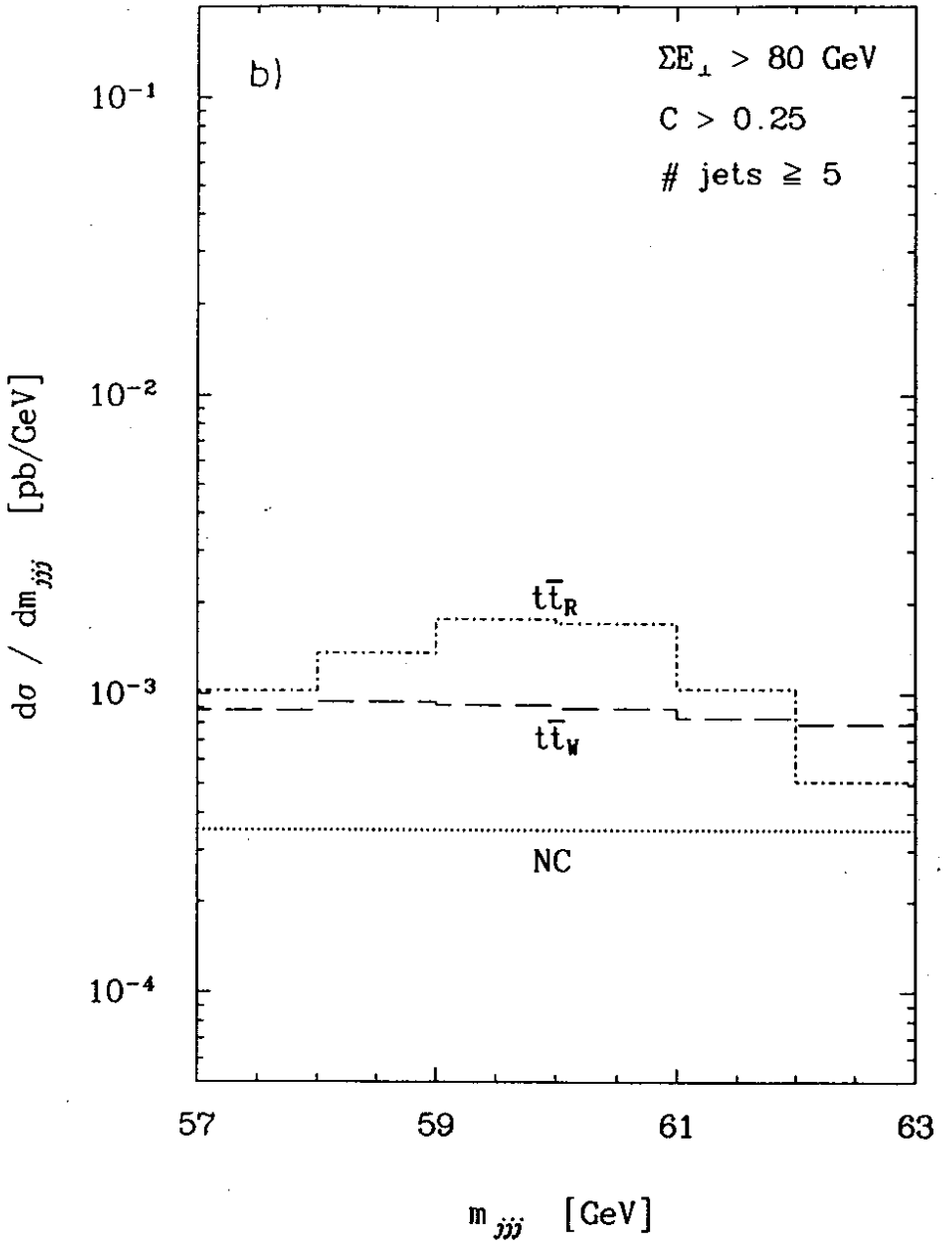

Figure 22 (b)